https://doi.org/10.5194/egusphere-2026-5202
Preprint. Discussion started: 9 September 2026

Convective environments prone to downbursts, large hail, short-duration precipitation extremes and tornadoes in Spain

Andres Barrio-Martin[1], Carlos Calvo-Sancho[1], Nuria P. Plaza-Martin[1], Cesar Azorin-Molina[1], Andreas F. Prein[2], Tim R. McVicar[3], Sergio M. Vicente-Serrano[4], Luis Gimeno[5], Raquel Nieto[5], Zhenzhong Zeng[6], Ana Morata[7] and Deliang Chen[8].

[1] Centro de Investigaciones sobre Desertificación, Consejo Superior de Investigaciones Científicas (CIDE, CSIC-UV-GVA), Climate, Atmosphere and Ocean Laboratory (Climatoc-Lab), Moncada, Valencia, Spain.
[2] Institute for Atmospheric and Climate Science, ETH Zürich, 8092 Zurich, Switzerland
[3] CSIRO Environment, Canberra, ACT 2601, Australia
[4] Instituto Pirenaico de Ecología, Consejo Superior de Investigaciones Científicas (IPE-CSIC), 50059 – Zaragoza, Spain
[5] Centro de Investigación Mariña, Universidade de Vigo, Environmental Physics Laboratory (EPhysLab), Ourense, Spain
[6] School of Environmental Science and Engineering, Southern University of Science and Technology, Shenzhen 518055, China
[7] Department of Science and Climatology, Spanish State Meteorological Agency, Madrid, Spain.
[8] Department of Earth System Science, Tsinghua University, Beijing 100084, People's Republic of China

Correspondence to: A. Barrio-Martin (andres.barrio@csic.es)

Abstract

Deep moist convection produces several hazards including downbursts, tornadoes, large hail, and short-duration precipitation extremes, resulting in fatalities and substantial economic losses. This study employs observational reports, lightning flashes and the ERA5 reanalysis over Spain (2015-2024) to summarize the key environmental differences between non-severe convection and each of these hazards, by ranking 203 convective parameters according to their discriminatory skill, and comparing composite vertical profiles. Summer downburst environments are markedly warmer than non-severe environments, with downdraft Convective Available Potential Energy (CAPE) emerging as the most discriminating parameter. Non-summer downbursts show enhanced wind shear relative to non-severe convection, though rarely reaching High-Shear–Low-CAPE conditions. Summer tornadoes and waterspouts display higher 0–3 km CAPE and a lower level of free convection than non-severe convection, but non-summer cases overlap substantially with non-severe environments. Hail over 5 cm in diameter occurs mostly in summer, in environments of elevated CAPE and shear, best distinguished by the WMAXSHEAR composite index. Short-duration precipitation extremes, evaluated during non-summer months, are associated with elevated moisture and some supercell signatures, supporting slow motions. These results provide a comprehensive framework for future studies on severe convective weather and climate model projections, representative of the Mediterranean severe convective environments.

Keywords: downbursts, tornadoes, large hail, short-duration precipitation extremes, ERA5, convective parameters, severe convection

https://doi.org/10.5194/egusphere-2026-5202
Preprint. Discussion started: 9 September 2026

1. Introduction

Deep moist convection can involve considerable hazards, including convectively induced winds (downbursts), tornadoes, large hail and/or short-duration precipitation extremes. Downbursts are capable of collapsing structures and uprooting trees, potentially risking human life and causing important damages (Solari, 2020). They accounted for 78 fatalities in Europe over 2009–2020, occurring as frequently as every other day on average (Pacey et al., 2021), and in Canada, they are the most disastrous wind type, causing ~67% of the total loss associated with windstorms (Hadavi et al., 2022). Other wind-related phenomena, tornadoes, are most frequent in the US, but their impacts are still noticeable worldwide, causing on average 5 fatalities, 70 injuries and more than €15 million in losses every year in Europe (Antonescu et al., 2017), while in China, the violent Yancheng tornado (23 July 2016) caused 99 fatalities and more than 800 injuries (Xue et al., 2016). Although not as lethal, hail results in much more widespread damage to crops and property (Battaglioli et al., 2026; Púčik et al., 2019; Schuster et al., 2005), and exceptionally giant hail up to 12 cm in diameter can produce fatalities (Martín et al., 2024). Lastly, the deadliest convective hazard corresponds to flash floods, which can be induced by short-duration precipitation extremes, in addition to many hydrological intricacies (Llasat et al., 2016; Doswell et al., 1996). For instance, on 29 October 2024 a flash flood in the Valencia region (Spain) accounted for 230 fatalities, devastated many infrastructures and caused economic losses of several billions of euros (Calvo-Sancho et al., 2026), and in the Indian Himalayas, rainfall intensities exceeding 100 mm h^{-1} localized in 20–30 km^2 can produce devastating impacts reaching 6,600 fatalities in single events (Dimri et al., 2017). Concerningly about these hazards, growing evidence supports that anthropogenic climate change enhances the frequency and intensity of both severe convective winds (Prein, 2023; González-Alemán et al., 2023; Pilguj et al., 2022; Walle et al., 2021) and hail (Battaglioli et al., 2023, 2026; Raupach et al., 2021), in addition to long term trend analyses (Merino et al., 2018), climate change projections (del Jesus and Diez-Sierra; 2023), and attribution approaches that have exposed its intensifying role of short-duration precipitation extremes leading to flash floods (Calvo-Sancho et al., 2026; Saurral et al., 2026; Walle et al., 2021).

The dynamics of severe convective weather are often intricate and highly localized (Markowski and Richardson, 2010; Doswell et al., 1996). Severe convective winds arise from downdrafts that impinge on the surface, covering a wide range of spatial scales from downbursts (<10 km) to derechos (>400 km). Although storm dynamics can induce vertical pressure-perturbation gradients contributing to downward acceleration, the primary forcings of convective winds are evaporative cooling and condensate loading, which generate negative buoyancy (modulated by environmental instability), as well as rear inflow jets, meso- and microscale vortices or the downward transport of horizontal momentum from aloft (Burlando and Romanic, 2021; Markowski and Richardson, 2010; Wakimoto, 2001). Tornadoes can form within a wide variety of storms, most often linked to rapidly developing cumulus that stretch the pre-existent vorticity along air-mass boundaries such as cold pools or land-sea interfaces. The most violent but least frequent tornadoes are associated with supercells and their mesocyclones. Convergence plays a key role in concentrating vertical vorticity, while downdrafts and updrafts tilt horizontal vorticity into vertical vorticity, which is further intensified through stretching (Clark and Smart, 2015; Davies-Jones, 2015; Doswell et al., 1993). Hail formation requires strong and sustained updrafts that allow continuous interactions among hydrometeors such as ice crystals, supercooled droplets, and graupel. Collision-coalescence processes enlarge hailstones, with their final size depending on the availability of liquid water and the residence time within layers rich in supercooled water. Large hail (> 5 cm) occurs almost exclusively in supercells, due to their persistent and intense updrafts (Allen et al., 2020; Trapp, 2013). Flash floods–considering only meteorological drivers–require persistent and/or heavy rainfall. Persistence is favored in back-building systems, where new convective cells repeatedly form over the same location, or in slow moving systems. Rainfall intensity is enhanced by abundant low-level moisture and strong updrafts, whereas environmental entrainment promotes evaporation and strong storm-

https://doi.org/10.5194/egusphere-2026-5202
Preprint. Discussion started: 9 September 2026

relative winds disperse hydrometeors over vast areas, reducing local accumulation (Houze Jr, 2014; Markowski and Richardson, 2010).

Because many severe weather hazards occur at scales unresolved by most atmospheric models, rather than using direct model outputs, such as modelled wind speed when diagnosing tornadoes, the model's resolved environmental characteristics are commonly processed into several convective parameters, which serve as proxies for severe weather (Doswell et al., 1996). Convective parameters are widely used in the research on convection and its associated hazards (e.g., Taszarek et al., 2020; Gensini and Ashley, 2011; Brooks et al., 2007; Kunz, 2007), and to assess trends and climatologies of convective environments from a global perspective (Battaglioli et al., 2026; Taszarek et al., 2021b). The applications of convective parameters include the characterization of environments leading to severe convective winds (Pacey et al., 2021, Europe; Bechis et al., 2025, South America; Romanic et al., 2022, US; Hadavi and Romanic, 2024a,b, Canada), tornadoes (Nixon et al., 2022, 2023, US; Novitskii et al., 2015, Russia), hail (Bhavyasree et al., 2026, India; Wang et al., 2026, Weining; Taszarek et al., 2020, Europe), or short-duration precipitation extremes (Burow et al., 2025; US). Severe weather environments are also often analyzed collectively, i.e., not distinguishing across the different hazards (Li et al., 2020; Gensini et al., 2014). There are a vast number of convective parameters and parameter formulations. Open-source sounding-processing software provides tens to hundreds of parameters for each profile (Czernecki et al., 2025; Blumberg et al., 2017), allowing the quantification of physically relevant aspects (e.g., storm-relative wind, freezing level). Nevertheless, using the totality of the available parameters is impractical in operational settings and, in machine learning applications (Chase et al., 2022), often requiring a prior selection.

Several studies find regional differences in severe weather environments, highlighting the need for local characterizations. For example, downburst environments in Canada differ from the United States both in terms of the most representative convective parameters and in weaker equivalent potential temperature deficits (Hadavi and Romanic, 2024a), and in South America the magnitudes of composite indices for severe weather show much lower values than suggested thresholds (Bechis et al., 2025). Moreover, complex orography can impact the environments leading to severe convection (Díaz-Fernández et al., 2025). Such regional characterization is particularly relevant for the Mediterranean, surrounded by complex orography, and where frequent severe convection events (Fery and Faranda, 2024; González-Alemán et al., 2023; Calvo-Sancho et al., 2022; Papavasileiou et al., 2022; Melani et al., 2013) are expected to increase in frequency and/or intensity by modelling and attribution approaches (Calvo-Sancho et al., 2026; Martín et al., 2024; Battaglioli et al., 2023; González-Alemán et al., 2023; Llasat et al., 2021). Yet, a comprehensive characterization of severe convective environments in the Mediterranean region is still lacking. An early precedent, Tudurí and Ramis (1997), classified environments for several hazards in the Balearic Islands using classic stability indices, which they found to poorly discriminate between event types. More recently, Taszarek et al. (2020), compared severe weather environments between Europe and the US, but the tendency of the Mediterranean region to underreporting limited its European domain to central Europe.

For these reasons, our objectives are: (i) to identify, among a wide set of convective parameters, those with the greatest discriminatory skill between each severe convective hazard and non-severe convection; and (ii) to characterize, using these parameters, the convective environments associated with severe weather over Spain, as a representative region in the western Mediterranean, with special emphasis on severe convective winds generated by downbursts, while also addressing tornadoes, large hail and short-duration precipitation extremes

This paper is organized as follows. Section 2 describes datasets and methods, including the definition of non-severe convection and each severe weather hazard, and the binary classification process. Section 3 contains the results and discussions of this

https://doi.org/10.5194/egusphere-2026-5202
Preprint. Discussion started: 9 September 2026

study, including the comparison between each hazard and non-severe convection in terms of the convective parameters with highest distinguishing skill and in terms of composite vertical profiles. Last, conclusions are drawn in Section 4.

2. Data and methodology

This section describes how severe weather observational reports, ERA5 reanalysis and cloud-to-ground lightning have been combined to construct a 2015–2024 sample of severe and non-severe convection, described in terms of convective parameters. These parameters have been sorted by their skill in distinguishing severe and non-severe environments, and composite profiles were produced. The methodology largely follows previous studies (Hadavi and Romanic, 2024a, 2024b; Nixon et al., 2023, 2022; Romanic et al., 2022), while also including some new approaches such as a refined selection of convective initiation times and geographical restraints on the comparison. These new approaches are detailed in full below.

2.1 Observational reports

The samples of severe convective weather covering 2015–2024 (Table 1) have been obtained from SINOBAS (sinobas.aemet.es; last accessed 22 May 2026), excepting large hail (derived from radar and citizen science; Martín et al., 2021). SINOBAS is a public dataset of observational reports, compiled by the Spanish State Meteorological Agency (AEMET), focused on localized severe weather phenomena across Spain (micro- and meso-gamma scales). In SINOBAS the level of detail varies from brief subjective estimations to comprehensive documentation including thermodynamic diagrams, radar imagery and/or synoptic descriptions. All SINOBAS reports include an estimated time and location, which are the key features used in this research. In addition, AEMET meteorologists often review, complete or elaborate the reports, assigning one of three confidence levels based on the available evidence (e.g. damages, weather stations, remote sensing). More than 95% of the events used herein correspond with high or medium confidence. We expect biases in SINOBAS towards urban areas, as rural areas contain a smaller density of potential observers, as with most report-based datasets (Hadavi and Romanic, 2024a; Romanic et al., 2022; Pîrloagă and Antonescu, 2021; Gayà, 2011).

Regarding severe convective winds, SINOBAS merges downbursts and gust fronts into a single category, while distinguishing heat bursts. Herein, all three cases were considered collectively due to the limited sample size. Regarding short-duration precipitation extremes, these are defined by convective heavy rainfall events, highly localized over small areas and having the risk of producing flash floods (see criteria in Table 1).

Table 1. Acronyms, criteria and source of convective events analyzed herein.

Events	Acronym	Criteria	Source
Downbursts and/or gust fronts (including heat bursts)	DWB	Estimated gusts over 80 km/h (and >5ºC rise for heat bursts)	SINOBAS
Tornadoes and waterspouts	TND	Visual	SINOBAS
Large hail	HAIL	Diameter greater than 5 cm	Calvo-Sancho et al. (2022), (Martín et al., 2023)
Short-duration precipitation extremes	PRCP	Duration between 30’ and 3 h, extending less than 50 km^2 and reaching 60 mm/h.	SINOBAS
Non-severe thunderstorms	Non-Sev	Further than 3º in latitude and longitude and ±6 h from any of the previous hazards	Cloud-to-ground lightnings (AEMET)

https://doi.org/10.5194/egusphere-2026-5202
Preprint. Discussion started: 9 September 2026

2.2 ERA5

ERA5 is the fifth-generation global reanalysis produced by the European Centre for Medium-Range Weather Forecast (ECMWF), generated by data assimilation techniques and provided at hourly resolution on a 0.25º grid (Hersbach et al., 2020). Reanalyses help to overcome the sparse spatial resolution of radiosonde stations and their limited frequency, typically restricted to 0000 and 1200 UTC, which can miss peak diurnal convection at some locations (Taszarek et al., 2020). The ERA5 reanalysis was used to extract vertical profiles of air temperature, specific humidity, pressure and both wind components, describing the large-scale environments associated with severe and non-severe convection over 2015–2024.

Regarding the vertical dimension, we use the native model levels of ERA5, despite the 37 standard pressure levels being more commonly used, as recommended in Taszarek et al. (2021b). Model levels offer an increased resolution (137 levels) and they adapt to the orography, unlike pressure levels, which is crucial for an accurate representation of inversions and rapid changes in the boundary layer, where 28 levels lie in 0–2 km from the model surface. Given our focus on convective parameters, it is important to note that the better representation of profiles in model levels has been shown to yield more accurate representations of buoyancy convective parameters (Varga and Breuer, 2022).

ERA5 has been validated as an overall valuable source of convective parameters, when compared to sounding observations (Taszarek et al., 2021b). Although many kinematic and thermodynamic parameters, associated with larger scales, are reasonably well represented, the agreement with soundings is less for parcel-based parameters or composite indexes (Varga and Breuer, 2022; Taszarek et al., 2021b).

2.3 Extracting severe and non-severe profiles

Cloud-to-ground lightning measurements were provided by AEMET, covering Spain for 2015–2024 with spatial accuracies of 100 meters and temporal precision of seconds (Núñez Mora et al., 2019). Lightning observations were used to derive a sample of gridded thunderstorms, that in turn is used to derive a null class of non-severe thunderstorms for comparison against each severe convective hazard, a common practice in severe weather characterization (Hadavi and Romanic, 2024a, 2024b; Romanic et al., 2022; Czernecki et al., 2019).

To extract the vertical profiles associated to severe thunderstorms and non-severe thunderstorms the next procedure was applied:

1. The locations and timings of lightning and severe reports were mapped onto the ERA5 grid. As our research focuses on pre-convective environments, consecutive lightnings were removed (i.e. in the same grid and less than 1 h apart), retaining only the first lightning in each sequence and grid, ensuring the representativity of the onset of convection rather than its mature or decaying stages.
2. For each gridded severe-weather report, we then searched for the first lightning flash occurring in the grid and the 8 neighboring grids within the previous 3 h, determining the time t_0 (Supplementary Fig. S1). Then, the ERA5 vertical profile was extracted at the grid of the report during the hour preceding t_0. If no lightning was found in this process, t_0 is set to the hour prior to the report. Overall, this step avoids collecting profiles no longer representative of pre-convective conditions due to the presence of nearby convection (i.e. within 45 km). It is also motivated by the possibility of hazards occurring during the mature or dissipating stages of mesoscale convective systems which can travel tens of kilometers before reaching the report location.

https://doi.org/10.5194/egusphere-2026-5202
Preprint. Discussion started: 9 September 2026

While more than 95% and 97% of PRCP and large hail were accompanied by lightning, respectively, downbursts can occur without nearby lightning (Hadavi and Romanic, 2024a), and the presence of lightning flashes was used to subclassify the downburst sample into subsequent analyses (Table 2). Although a substantial fraction of waterspouts and tornadoes (29%) also occur without lightning, their detailed subclassification falls beyond the scope of this research.

3.To label non-severe events, we excluded all the lightning flashes within 6 h and 3º in latitude and longitude of any severe report.

Table 2. Subclassification of downburst environments based on their distance to cloud-to-ground lightning.

Downburst subclass	Number and accumulated (%)	Are there cloud-to-ground lightning?
Close to lightning	126 (66%)	Yes, in the report grid, 0–3 h from the report
Far from lightning	29 (82%)	Not in the report grid, but in the 8 surrounding ones, 0–3 h from the report
No lightning	35 (100%)	None of the above

The spatial distribution of severe reports and non-severe thunderstorms is shown in Fig. 1. Mountains are sparsely populated areas that are particularly prone to underreporting. For instance, the eastern local maxima of 400, 300 and 200 thunderstorms in Fig. 1e, corresponding to mountainous areas, show few downburst or tornado reports (Fig. 1a,c), despite frequent thunderstorm occurrences likely enhanced by orographic lifting (Núñez Mora et al., 2019; Kirshbaum et al., 2018). For this reason, we applied a geographical restraint, which is described in Sect. 2.5 and is intended to retain the differences arising from the atmospheric environments specific to severe convection, rather than from climatological differences synthetically arising from reporting biases.

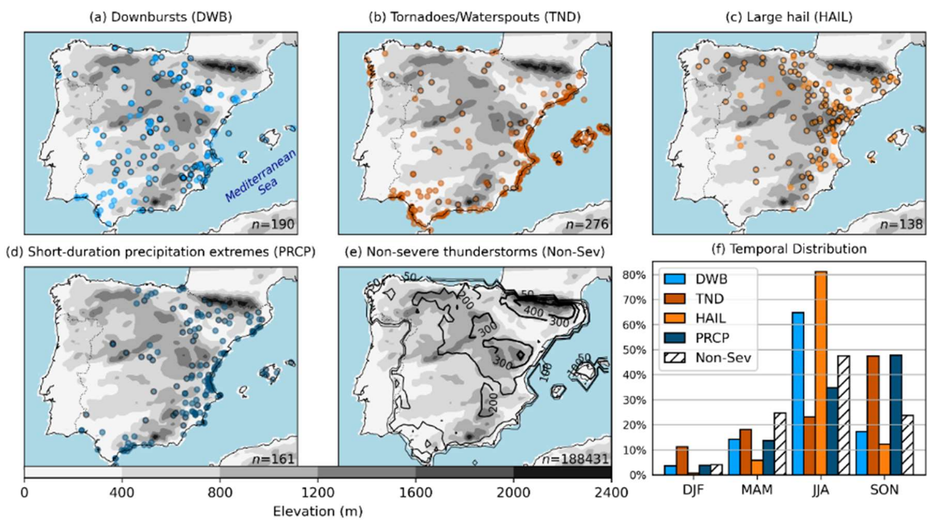

Figure 1. Spatiotemporal distribution of the samples studied herein. (a-d) Spatial distribution and number (*n*) of the different severe weather reports, with black-outlined circular markers highlighting summer events. Topography gray-shaded each 400 m. (e) Contours denoting the number of non-severe thunderstorms over 2015–2024. (f) Relative seasonal frequency of each severe weather hazard and non-severe thunderstorms. Domain: 10º W–5º E, 35º N–45º N.

https://doi.org/10.5194/egusphere-2026-5202
Preprint. Discussion started: 9 September 2026

2.4 Convective parameters

The vertical profiles of ERA5 were processed using the thundeR software (Czernecki et al., 2025), which computes 201 convective parameters for each event. In addition, GUSTEX (Dotzek and Friedrich, 2009) and the Downburst Precursor Parameter (Hadavi and Romanic, 2024a) were computed and included in our research (further information in Table 3). Table 3 shows the most relevant parameters for our subsequent analysis (Sect. 2.5), but all the 203 parameters were tried. We finally excluded the significant tornado parameter and the altitude of maximum equivalent potential temperature, because their tendency to zero values resulted in errors for our methodology.

Table 3: Convective parameters from thundeR appearing in this manuscript. All altitudes are expressed with respect to ground level. There are four parameter categories, indicated in *italics*. [a] There are three types of low-level parcels: SB (surface-based), ML (mixed-mayer) and MU (most-unstable). If applicable, their acronyms are appended to the parameter. [b] Many parameters depend on a given layer. If applicable, the layer is appended to the parameter. [c] Certain parameters assume a supercell motion vector computed using the method of Bunkers (2000), which is indicated by RM (right-mover, cyclonic) and LM (left-mover, anticyclonic). For full details, see Czernecki et al. (2025).

Parameter	Formulations	Description
Parcel-based parameters		
LCL	SB, ML [a]	Level of Condensation by Lifting.
LFC (Temperature)	MU [a]	Level of Free Convection altitude (or its temperature).
Mixing Ratio	ML[a]	Water vapor mixing ratio of the parcel.
Lifted Index	ML [a]	Temperature difference between the environment and the ascending parcel at 500 hPa.
CAPE	ML [a] over -10ºC level, 0–3 km [b]	Convective Available Potential Energy.
CIN	SB [a]	Convective INhibition.
DCAPE	–	Downdraft Convective Available Potential Energy, computed for a parcel with mean θ_e over 3–5 km that descends pseudo-adiabatically from 4 km.
Thermodynamic Parameters		
Freezing Level (wet-bulb)	–	Height of the 0°C (wet-bulb) isotherm or melting layer.
Lapse Rate	0–1 km, 0–4 km [b]	Environmental temperature lapse rate. Rate of decrease of temperature with altitude.
Relative Humidity	0–2 km, 3–6 km [b]	Mean relative humidity over a layer.
Precipitable Water	–	Column integrated water vapor.
Moisture Flux	0–2 km [b]	Product of wind speed multiplied by mixing ratio.
θ_e	0–1 km [b]	Equivalent potential temperature.
$\Delta\theta_e$	–	θ_e deficit between mid-levels (3–5 km) and surface.
Kinematic arameters		
Shear	0–1 km, 0–6 km, surface to -10 ºC, ML LFC to -10 ºC [b]	Bulk vertical wind shear over a layer.
Shear: Effective	ML, MU [a]	Bulk wind shear between the LCL and half of its distance to the equilibrium level of the ascending parcel (Thompson et al., 2007).
Streamwise vorticity	0–1 km [b] RM [c]	Component of the storm-relative vorticity vector that is parallel to the horizontal wind direction.
Storm-relative helicity	0–100 m, 0–1 km [b] RM, LM [c]	Potential for updraft rotation, defined by the vertical integral of streamwise vorticity weighted by storm-relative wind speed.
Mean Storm Motion (Azimuth)	–	Ground-relative storm motion speed (direction), using the method of Bunkers (2000).
Bunkers	RM [c]	Speed of a supercell, using the method of Bunkers (2000).
Corfidi Downwind Motion	–	Speed of downwind-propagating mesoscale convective systems (Corfidi, 2003).

https://doi.org/10.5194/egusphere-2026-5202
Preprint. Discussion started: 9 September 2026

Composite indices		
Downburst Environment Index	–	Linear combination of Cold Pool Strength and WMAXSHEAR (see below), indicating downburst-prone environments (Romanic et al., 2022).
Downburst Precursor Parameter	–	Linear combination of $\Delta\theta_e$ and Shear: Effective ML, specifically designed for Canada (Hadavi and Romanic., 2024a).
Wind Index	–	Wind gust estimation for microbursts based on the freezing level, and temperature and moisture at low-to-mid levels (McCann, 1994).
GUSTEX	–	Wind gust estimation, including downward transport of horizontal momentum. Computed as the average of Wind Index and the mean wind over 1–5 km. (Geerts, 2001).
Hail Size Index	–	Estimate of hail growth potential (Czernecki et al., 2019).
Significant Hail Intensity Parameter	–	Composite index for large hail (Storm Prediction Center, 2021).
WMAXSHEAR	WMAX: ML [a] Shear: 0–6 km, ML effective layer [b]	Maximum updraft speed (WMAX) of the parcel multiplied by 0–6 km shear (Taszarek et al., 2017).
WMAXSHEAR: Effective	WMAX: ML [a] Shear: ML effective layer [b]	Maximum updraft speed (WMAX) of the parcel multiplied by effective shear (see above).
Energy Helicity Index	Helicity: 0–3 km [b] RM, LM [c]	Product of CAPE and helicity (Hart and Korotky, 1991).
Supercell Composite Parameter	–	Normalized product of CAPE, 0–3 km storm-relative helicity, effective shear and inverse of CIN (Gropp and Davenport, 2018)
SHERBS3	–	Severe Hazards in Environments of Reduced Buoyancy parameter (Sherburn and Parker, 2014). Product of Lapse Rate 0–3 km, Shear 0–3 km and the maximum 2 km lapse rate between 2 and 6 km.
K Index	–	Thunderstorm potential index, depending on lapse rate, moisture content of the lower atmosphere, and depth of the moist layer (George, 1960).
Total Totals Index	–	Thunderstorm potential index, based on the temperature lapse rate in the 850–500 hPa layer and the 850 hPa dewpoint (Miller, 1972).
Showalter Index	–	Atmospheric stability index, with negative values indicating instability (Showalter, 1953).

2.5 Comparison between severe and non-severe thunderstorms

For the comparison between severe and non-severe thunderstorms, two temporal aggregations were considered: summer (1-June to 31-August) and non-summer (1-September to 31-May). This choice is motivated by previous studies showing that severe convective environments differ substantially between warm and cold seasons, typically corresponding to High-CAPE-Low-Shear (HCLS) and High-Shear-Low-CAPE (HSLC), respectively (Púčik et al., 2015; Corfidi et al., 2006; Evans and Doswell III, 2001). Accordingly, these regimes are associated with distinct physical mechanisms. For example, severe convective winds in warm environments are more often linked to negative buoyancy and isolated cells, whereas in colder environments they tend to arise from organized systems capable of generating their own mesoscale dynamics (Pacey et al., 2021). The chosen aggregation therefore allows us to assess whether similar seasonal distinctions emerge here. Under this aggregation, reduced sample sizes for summer PRCP (58 cases) and non-summer large hail (26 cases) lead to statistically poor results, so these categories were excluded. Summer tornadoes (67 cases) were also limited in number but they are shown because of their physically more reliable patterns than non-summer tornadoes.

In addition, the comparison of each of these severe weather samples with non-severe convection was performed using only the locations of the severe sample being compared, and excluding all other non-severe samples. This geographical restraint had the objective of reducing biases arising from unreported severe weather in sparsely populated areas, as discussed in Sect. 2.1 and 2.3. The logic behind is that, if severe weather has already been reported in some grid, it is likely that there are either a considerable number of potential observers and/or automated weather stations, potentially reducing the number of unreported events.

https://doi.org/10.5194/egusphere-2026-5202
Preprint. Discussion started: 9 September 2026

The differences between severe and non-severe environments were assessed using two complementary approaches. Firstly, a binary classification designed to identify the convective parameters with the greatest distinguishing skill. This is achieved through Receiver Operating Characteristic (ROC) curves and their associated metric, the Area Under the Curve (AUC), which has been widely used in similar studies to quantify discriminatory performance (Hadavi and Romanic, 2024a; Romanic et al., 2022; Sherburn and Parker, 2014). ROC curves were computed following the contingency table defined in Table 4. A key challenge arises from the markedly unbalanced sample sizes between severe and non-severe environments, on the order of 100:10 000. Thus, to enhance statistical robustness, we applied a bootstrapping procedure in which random non-severe subsets of equal size to the severe sample were repeatedly drawn 1,000 times, finally averaging all the ROC curves and their corresponding AUC values, and computing its standard deviation (σ). Parameters with AUC values close to 1 (close to 0) can be interpreted as having a strong distinguishing skill, indicating that severe environments tend to have systematically higher (lower) values. Conversely, AUC values close to 0.5 indicate poor discriminatory ability, reflecting a high rate of false positives and false negatives for every possible threshold in the convective parameter. For interpretability, parameters with AUC values below 0.5 were transformed to fall within the 0.5–1 range, by inverting the inequalities in Table 4, which has been indicated as "higher values for non-severe thunderstorms" throughout Sect. 3. Lastly, to avoid repeating the same parameter under different formulations and to provide a comprehensive environmental characterization, we keep only the best formulation of each parameter and the two best parameters of each category among the complete pool of convective parameters.

Table 4. Contingency table used for the ROC curve calculations. Each value of the sample for the convective parameter (x) being evaluated is used as a threshold x_0 to construct points in the curve (FPR, TPR). Finally, ROC curves are linearly interpolated following a 0.05 spacing in FPR and AUC is computed using trapezoid integration.

Threshold at x_0	Number of x greater than x_0	Number of x less than x_0	Rates
Severe sample	True Positives (TP)	False Negatives (FN)	True Positive Rate TPR=TP/(TP+FN)
Non-severe sample	False Positives (FP)	True Negative (TN)	False Positive Rate FPR=FP/(FP+TN)

Compositing vertical profiles was the second method to assess the differences between severe and non-severe environments. For composite skew-T diagrams, we took the median of temperature and dewpoint profiles across all events, and the interquartile range was used to measure dispersion. For composite hodographs, we took the median of both wind components. However, as noted by Nixon and Allen (2022), similarly shaped hodographs may differ substantially in orientation and cancel out. Therefore, following that study, we adopted a second compositing strategy that preserves the shape of hodographs, independently of the prevailing wind directions: first, the surface wind vector was first subtracted; then, the profiles were rotated such that the 0–3 km shear vector aligned with the new u-component axis and, finally, we took the median of the new wind components at each level.

https://doi.org/10.5194/egusphere-2026-5202
Preprint. Discussion started: 9 September 2026

3. Results and discussion

3.1 Downbursts

3.1.1 Summer downbursts

The convective parameters that best distinguish between summer downbursts and non-severe thunderstorms are listed in Table 5. The AUC values scored in the classification indicate moderate skill (0.78–0.80; AUC ranges from 0.5 to 1), highlighting the inherent difficulty of separating both environments. Considering the four categories of convective parameters, the AUC ranking in Table 5 is dominated by parcel-based, thermodynamic and composite parameters, while kinematic parameters offer little discriminatory power.

Table 5. Ranking of the best convective parameters for classifying summer downburst environments. Each parameter-AUC set presents the results for accumulated downburst subsamples (close, far or in absence of nearby lightnings; Sect. 2.2). DCAPE: Downdraft Convective Available Energy; LCL: Level of Condensation by Lifting; SRH: storm-relative helicity; RM: right-mover motion; SB: surface-based parcel; ML: mixed-layer parcel. [a] Higher values for non-severe thunderstorms.

Close to lightning		Close/far from lightning		Close/far/no lightning	
Parameter	AUC (σ)	Parameter	AUC (σ)	Parameter	AUC (σ)
Downburst Environment Index	0.78(.03)	Cold Pool Strength	0.75(.03)	DCAPE	0.80(.02)
Wind Index	0.77(.03)	Wind Index	0.75(.03)	Freezing Level	0.77(.02)
Cold Pool Strength	0.76(.03)	Downburst Environment Index	0.74(.03)	Relative Humidity 0–2 km	0.75(.02)[a]
Lapse Rate 0–1 km	0.73(.03)	DCAPE	0.71(.03)	Downburst Environment Index	0.73(.02)
DCAPE	0.70(.03)	Lapse Rate 0–4 km	0.71(.03)	ML LCL	0.72(.02)
SB LCL	0.70(.03)	SB LCL	0.70(.03)	Wind Index	0.70(.02)
Shear 0–1 km	0.64(.03)	Shear 0–1 km	0.61(.03)	SRH 100 m RM	0.58(.03)
Streamwise Vorticity 0–1 km RM	0.61(.04)	SRH 1 km RM	0.60(.03)	Mean Wind: 0–500 m	0.57(.03)

For downbursts close to lightning, the most important parameters are downburst composite indices (Wind Index and Downburst Environment Index), but in the most general sample, thermodynamic and parcel parameters become more relevant (close/far/no lightning; Table 5). Including downbursts far or lacking nearby lightning increases the overall distinction from non-severe environments, with DCAPE achieving the highest AUC in the full sample. The ROC curves in Fig. 2 illustrate these changes, with all downburst cases improving the performance of Freezing Level and DCAPE in FPR ranges of 0–0.4, while reducing the performance of the Downburst Environment Index and Wind Index for FPR in range 0.6–1. This shift suggests that thermodynamic parameters provide more consistent discriminatory skill across the full spectrum of downbursts, while composite indexes are more sensitive to the presence of nearby lightning.

https://doi.org/10.5194/egusphere-2026-5202
Preprint. Discussion started: 9 September 2026

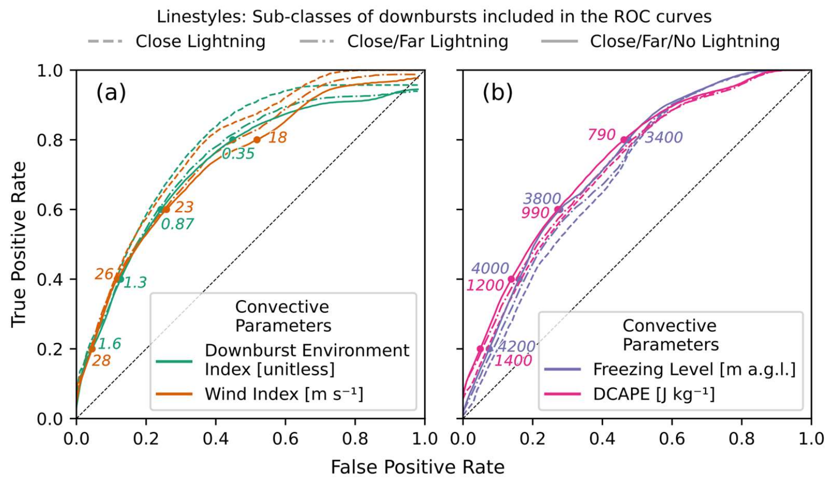

Figure 2: Receiver Operating Characteristic curves of selected parameters across progressively more general subclasses of summer downbursts. The numerical values annotated correspond to the lower thresholds in each convective parameter that are exceeded by 80%, 60%, 40% and 20 % of downbursts (i.e., true positive rates); only for the full downburst sample. DCAPE: Downdraft Convective Available Energy.

Figure 3 shows the comparison between downbursts and non-severe environments in terms of the distributions of several convective parameters, and Fig. 4 shows the vertical profiles they are computed from. Compared to non-severe convection, downburst environments are characterized by elevated values of DCAPE, Freezing Level and θ_e 0–2 km (Figs. 3a,b,e), together with steep lapse rates at mid-levels (Figs. 3g,h) that further enhance both CAPE and DCAPE (Figs. 3a,k). They also exhibit reduced 0–2 km mean relative humidity and an elevated LCL (Figs. 3c,f). These features result from the two main differences in the profiles of downbursts, with respect to non-severe convection: pronounced warmth and unsaturation, forming an inverted-V shape in skew-T diagrams (Fig. 4). The elevated values of DCAPE, Freezing Level and θ_e result from this warmth, which is concentrated in the lowest 0–3 km, explaining the steep lapse rates between this layer and mid-level layers. Reduced relative humidity and elevated LCL reflect unsaturation over the lower troposphere, evidenced by large dewpoint depressions over 0–3 km. This unsaturation is a consequence of the high air temperatures rather than low specific humidity, as shown by the similarity between downbursts and non-severe thunderstorms in their dewpoint profiles and moisture flux (Figs. 3j and 4).

Composite indices, although not achieving the greatest discriminatory skill, still must be acknowledged by their interpretability. That is, the Downburst Environment Index is centered at 0 for non-severe thunderstorms, while showing mostly positive values for downbursts (Fig. 3e), and the Wind Index estimates gust speeds that meet the criteria of observational reports (> 22 m s^{-1}) for 70% of downburst events (Fig. 3i).

https://doi.org/10.5194/egusphere-2026-5202
Preprint. Discussion started: 9 September 2026

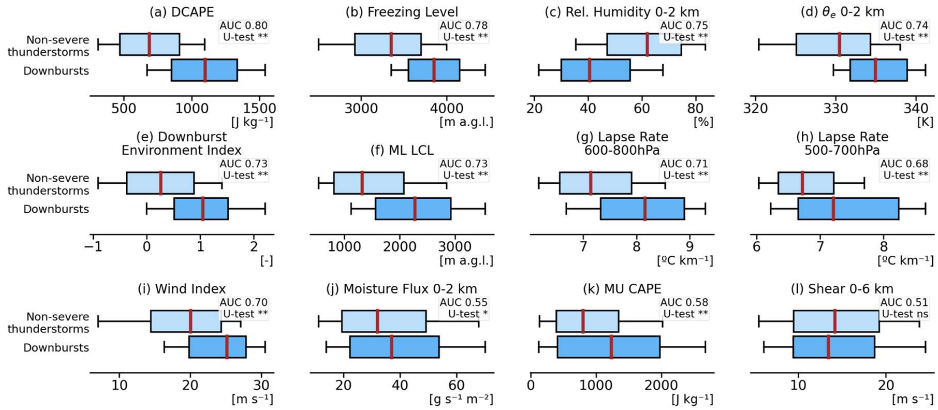

Figure 3: Box-and-whiskers plots of selected parameters for summer downbursts (dark blue boxes) and non-severe summer thunderstorms (light blue boxes). Boxes span the interquartilic range (IQR), whiskers extend to the 10th and 90th percentiles, and red horizontal lines indicate medians. AUC values for each parameter are provided. Mann-Whitney U-tests evaluate if both distributions differ for various confidence levels (ns: below 0.95; *: 0.95; **: 0.99). θ_e: equivalent potential temperature. ML: mixed-layer parcel. MU: most-unstable parcel. LCL: level of condensation by lifting. Descriptions of each parameter are provided in Table 3.

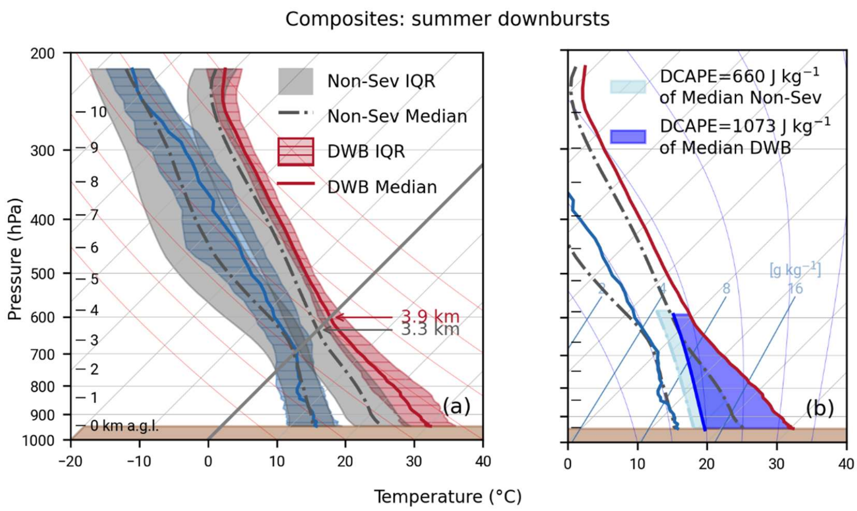

Figure 4: Composite skew-T/log-p diagrams for summer downburst (DWB; colored lines and shadings) and non-severe thunderstorms (Non-Sev; grey lines and shadings). (a) Median profiles and interquartile range (IQR). Red is used for the temperature and blue for the dewpoint downburst profiles. Altitude is relative to the average ground level. The 0 °C isotherm is highlighted and its intersection with the median profile is annotated showing the freezing level. (b) DCAPE shaded area associated with both median profiles.

The fact that DCAPE results the best classifier instead of dedicated indices, such as the Downburst Environment Index (Romanic et al., 2022), the Downburst Precursor Parameter (Hadavi and Romanic 2024a) or the Wind Index (McCann, 1994), suggests that these could be too tailored to the US/Canada, and they can be outperformed by other convective parameters in other regions. For example, in Australia, the Wind Index performs poorly when compared to many other parameters (Brown

https://doi.org/10.5194/egusphere-2026-5202
Preprint. Discussion started: 9 September 2026

and Dowdy, 2021) and, in South America, 0–3 km storm-relative wind discriminates between convective wind severity better than indices (Bechis et al., 2025). In addition to differences in the top-classifiers across regions, some convective parameters also exhibit substantial variability. DCAPE values are higher in Spain (IQR = 800–1300 J kg^{-1}) than in regions such as the US (500–900 J kg^{-1}; Romanic et al., 2022), China (400–800 J kg^{-1}; Huang et al., 2024) or South America (500–1000 J kg^{-1}; Bechis et al., 2025). We acknowledge different computations methods in the latter two cases, and that southwestern environments that lack in Romanic et al. (2022), resembling an arid environment closer to Spain, might be more similar. In addition to DCAPE, our lapse rates also exhibit differences with previous studies. Caplan et al. (1990) found that instability was crucial for dry microbursts in the US, with most of them associated with 500–700hPa lapse rates over 8 ºC km^{-1}. In contrast, our most representative layer is located between 600–800 hPa (Fig. 3g,h), and only 32% of our downbursts exceeded 8 ºC km^{-1} in the 500–700 hPa layer (55% in the 600–800 hPa layer), according with the central European environments of Pacey et al. (2021) also falling well below that threshold.

Physically, the lack of skill of kinematic parameters suggests that summer downbursts in Spain are primarily driven by thermodynamic forcings, with negative buoyancy playing a key role, agreeing with Srivastava (1987) and Wakimoto (1985). Therefore, less importance is expected from dynamical processes arising from pressure perturbations, such as in supercell occlusion downdrafts (Wakimoto 2001), although high-resolution simulations would be necessary to assess this statement (El Rafei et al., 2025). The high temperatures we found promote elevated freezing levels that may allow downward acceleration to accumulate over a deeper layer, as the freezing level often marks the initiation height of downdrafts (Dotzek and Friedrich, 2009; Knupp, 1989). Some case-studies have documented downbursts in Spain occurring during or immediately after heat waves resulting from southerly advection from North Africa, that promoted instability (Azorin-Molina, 2005; Arús Dumenjo, 2001).

The inverted-V shape in the composite downburst profile (Fig. 4) is a well-established signature of dry downbursts in unsaturated environments (Wakimoto, 2001, 1985). As discussed by James and Markowski (2010), low relative humidity can inhibit downdrafts, yet it is also often correlated with steep lapse rates having the opposite effect by enhancing negative buoyancy. These competing influences make it difficult to isolate the role of relative humidity alone. This discussion is relevant in our case, as the average 0–2 km relative humidity skillfully distinguishes downbursts from non-severe convection, but shows a strong correlation with both Lapse Rate 2–4 km and DCAPE (Spearman correlation coefficients of -0.80 and -0.81, respectively, > 99% significance).

3.1.2 Non-summer downbursts

Outside summer, the kinematic parameters emerge as the leading classifiers between downbursts and non-severe thunderstorms (Table 6, Fig. 5), in clear contrast with the thermodynamic importance in summer. The best classifier is wind shear from the surface to the -10ºC isotherm, and the most important composite index is SHERBS3, which measures potential severity in HSLC environments. Compared to the acceptable/good classification of summer downbursts, the non-summer classification achieves only a fair result, with maximum AUC of 0.69 against 0.80 in summer, and greater dispersion in the bootstrap (standard deviations up to 0.04 in AUC).

https://doi.org/10.5194/egusphere-2026-5202
Preprint. Discussion started: 9 September 2026

Table 6: Ranking of the best convective parameters for classifying non-summer downbursts against non-severe thunderstorms. *n* indicates the sample size ratio of both samples. MU: most unstable parcel. SB: surface-based parcel. SHERBS3: Severe Hazards in Environments with Reduced Buoyancy parameter using Shear 0–3 km. [a] Higher values for non-severe thunderstorms.

Non-summer downbursts classifiers n = (67:12205)	AUC (σ)
Shear: surface to -10ºC	0.69(.03)
Mean Storm Motion	0.67(.03)
SHERBS3	0.67(.03)
MU 0–2 km CAPE	0.65(.02)[a]
Total Totals Index	0.65(.04)[a]
Moisture Flux 0–2 km	0.64(.03)
Freezing Level (wet-bulb)	0.61(.03)
SB CIN	0.57(0.03)[a]

Non-summer downburst environments feature strong mid-level wind shear, when compared to the non-severe class (Fig. 5a,b,d), and exhibit lower CAPE than in summer (Figs. 3l and 5h), fulfilling the criteria of HSLC environments in some instances. Downburst indices and DCAPE, which were skillful classifiers in summer, exhibit now a poor performance (Fig. 5e-g), being outperformed by HSLC severity composite indices (Fig. 5c). Consistently, the composite skew-T diagram of non-summer downbursts is similar to that of non-severe thunderstorms (Fig. 6a), and the major differences are instead longer hodographs for downbursts than for non-severe thunderstorms (Figs. 6b,c). The increase in hodograph length is primarily associated with the 0–3 km layer (approximately -10ºC isotherm layer; Fig 5a) at which shear-based formulations achieve their highest AUC.

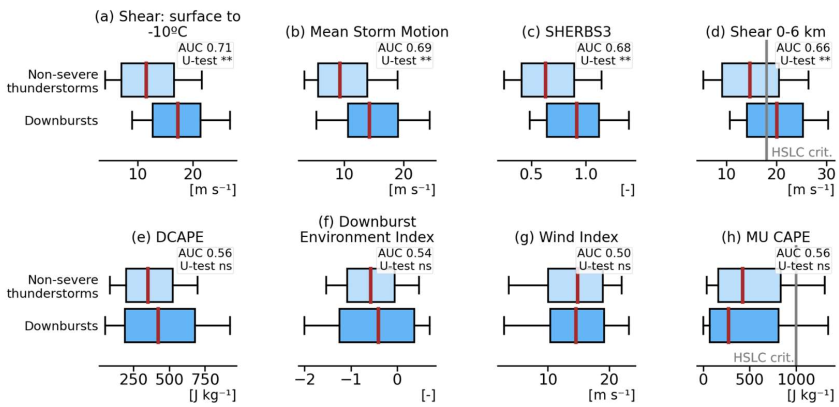

Figure 5: Box-and-whiskers plots of selected parameters for non-summer downbursts (dark blue boxes) and non-severe summer thunderstorms (light blue boxes). Boxes span the interquartilic range (IQR), whiskers extend to the 10th and 90th percentiles, and red horizontal lines indicate medians. AUC values for each parameter are provided. Mann-Whitney U-tests evaluate if both distributions differ for various confidence levels (ns: below 0.95; **: 0.99). In (d,h) High-Shear-Low-CAPE (HSLC) criteria are represented; they must be met simultaneously for an event and also require surface-based CAPE < 500 J kg^{-1}. MU: most unstable parcel. SB: surface-based parcel. SHERBS3: Severe Hazards in Environments with Reduced Buoyancy parameter using Shear

https://doi.org/10.5194/egusphere-2026-5202
Preprint. Discussion started: 9 September 2026

0–3 km.

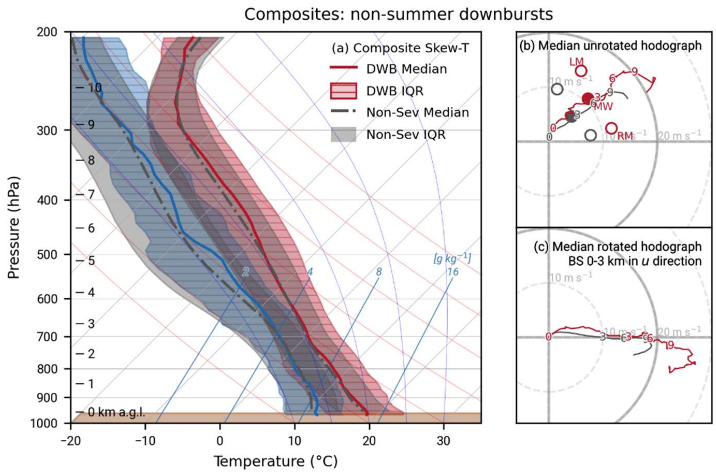

Figure 6: Composite profiles for non-summer downbursts (DWB; colored lines) and non-severe thunderstorms (Non-Sev; grey lines). (a) Composite skew-T. (b) Median hodograph with 3, 6 and 9 km altitudes annotated, also including motion vectors of right-mover supercells (RM), left-mover supercells (LM) and the mean 0–6 km wind (MW). (c) Shear-relative composite hodograph, with the origin of single profiles shifted to the center of the hodograph and 0–3 km bulk shear (BS) aligned with the wind *u*-component (i.e., eastward).

Physically, elevated wind shear can enhance several mechanisms responsible for severe convective winds, such as the downward transport of horizontal momentum from aloft or the development of misovortex circulations (Markowski and Richardson, 2010). These processes are usually associated with mesoscale convective systems that are also favored by strong shear (Dotzek and Friedrich, 2009; Geerts, 2001; Fujita, 1985). Consequently, strong vertical wind shear and storm organization often increase the chances of severe convective winds, such as in quasi-linear convective systems (QLCS) in the cold season (Pilguj et al., 2025).

Kinematic parameters consequently are frequently found as top-classifiers for cold-season convective winds in other studies (Hadavi and Romanic, 2024a; Pacey et al., 2021; Taszarek et al., 2020), but our results reveal large differences in the values of kinematic parameters, even from studies in the same continent. Although our downburst environments show stronger wind shear relative to non-severe environments, they remain weaker than central European cold-season environments. For instance, the median 0–6 km shear associated with European cold-season severe convective winds in Pacey et al. (2021) is 30 m s^{-1}, compared with 20 m s^{-1} in our downburst sample (Fig. 5d). Our median of 14 m s^{-1} for 0–6 km mean wind (mean storm motion; Fig. 5b) is already lower than the median of ~18 m s^{-1} associated with least severe QLCS as classified by Pilguj et al. (2025). Additionally, cold season severe convective winds typically develop in HSLC environments over Europe (Taszarek et al., 2020; Gatzen, 2018; Púčik et al., 2015), but only 40% of our non-summer downbursts meet the HSLC criteria of Sherburn and Parker (2014). This proportion is only slightly higher than the 25% found in non-severe environments, which is primarily due to relatively low shear in Spain (Fig. 5d).

A possible offset concerning the weak shear in non-summer downbursts may be given by DCAPE moderate values. For instance, in the cold-season environments of Pacey et al. (2021), roughly 25% of their cases exceed 300 J kg^{-1}, whereas this

https://doi.org/10.5194/egusphere-2026-5202
Preprint. Discussion started: 9 September 2026

threshold is exceeded by 61% of our samples (Fig. 5e). This suggests that downward acceleration may be compensating for the lack of such strong horizontal momentum aloft, allowing downbursts to occur despite weaker shear. Moreover, this appears to be a climatological feature of Spain, as downbursts and non-severe thunderstorms exhibit identical DCAPE distributions (U-test, $p < 0.05$; and Fig. 5e).

3.2 Tornadoes and waterspouts

3.2.1 Summer tornadoes and waterspouts

Table 7 lists the best classifiers between summer TND and non-severe thunderstorms. Their skill to classify both environments is only fair, with a maximum AUC of 0.69. Moreover, a parameter typically associated with tornadic environments, storm-relative helicity, performs poorly as a TND classifier (Fig. 7a,d). On the contrary, TND environments are best discriminated by elevated values of 0–3 km CAPE (Fig. 7a,b), in agreement with levels of free convection near the surface (Fig. 7c) that, in turn, yield elevated shear from the level of free convection to -10 ºC (Fig. 7e). A discrepancy occurs between the K index and $\Delta\theta_e$ indicate lower and greater instability than in non-severe events, respectively (Table 7).

Table 7. Ranking of the best convective parameters for classifying tornadoes/waterspouts (TND) against non-severe thunderstorms. *n* indicates the sample size ratio of both samples. ML: mixed-layer parcel. MU: most-unstable parcel. LFC: level of free convection. $\Delta\theta_e$: equivalent potential temperature deficits from mid-levels to surface. WMAXSHEAR: product of maximum updraft velocity and vertical shear. LCL: level of condensation by lifting. LFC: level of free convection. [a] Higher values for non-severe thunderstorms.

Summer TND n = (66:9615)	AUC (σ)	Non-summer TND n = (211:14293)	AUC (σ)
ML 0–3 km CAPE	0.69(.04)	K Index	0.62(.02)[a]
MU LFC	0.68(.04)[a]	Lapse Rate 600–800 hPa	0.62(.02)[a]
Relative Humidity 3–6 km	0.64(.03)[a]	Showalter Index	0.62(.02)
Shear: ML LFC to -10ºC	0.63(.03)	Shear: MU LFC to -10ºC	0.61(.02)
$\Delta\theta_e$	0.62(.03)	MU LCL	0.60(.02)[a]
K Index	0.61(.03)[a]	Corfidi Downwind Motion	0.59(.02)
ML WMAXSHEAR	0.57(.04)	MU LFC	0.59(.02)[a]
Mean Storm Motion Azimuth	0.53(.03)	Relative Humidity 0–1 km	0.58(.02)

The comparison across TND and non-severe profiles shows only slightly greater instability in the 0–3 km mean profile for TND, as denoted by the median temperature lapse rate (Fig. 8a). Above this layer, moisture content is reduced for TND. Regarding composite hodographs (Fig. 8b,c), the rotation of profiles before compositing appears to be crucial to preserve their shape. However, even after applying the shear-relative rotation, the resulting hodographs over 0–6 km exhibit minimal differences between TND and non-severe environments, and there are no signs of curvature or other typical shapes of TND in hodographs. Over 6–9 km, TND exhibits deeper shear.

Physically, one of the main contributors to tornadogenesis, the tilting term leading to supercells (Davies-Jones, 2015), might not be as crucial for our sample as other mechanisms, as suggested by the limited discriminatory skill of storm-relative helicity (Fig 7a), as well as the Energy Helicity Index or the Supercell Composite Parameter (AUCs of 0.50 and 0.52, respectively). Instead, alternative tornadogenesis processes rely on the stretching of pre-existent vertical vorticity along air-mass boundaries, often leading to less intensity tornadoes than those in supercells (Markowski and Richardson, 2010; Wakimoto and Wilson, 1989). Stretching benefits from near-surface strong updrafts, and the prevalence of this mechanism over stretching is suggested by 0–3 km CAPE leading the TND classification ranking, agreeing with Groenemeijer and Van Delden (2007). Overall, our

https://doi.org/10.5194/egusphere-2026-5202
Preprint. Discussion started: 9 September 2026

0–3 km CAPE distribution agrees with that of Taszarek et al. (2020), for F0-F1 Fujita scale intensity tornadoes, showing IQRs of 20–100 J kg^{-1}. Although 67% of our TND are not F-scale rated, previous climatologies showed that most tornadoes in Spain are precisely F0-F1 intensity (Rodríguez and Bech, 2021; Gayà, 2011). Our environments also match closely those associated with EF0 Enhanced Fujita scale intensity of Rodríguez and Bech (2018) in 0–1 km storm-relative helicity, with IQR of 10–50 m^2 s^{-2}. On the contrary, it is unclear that the reduced relative humidity in our TND profiles accounts for any physical mechanism relevant to tornadogenesis and might result from the reduced sample size.

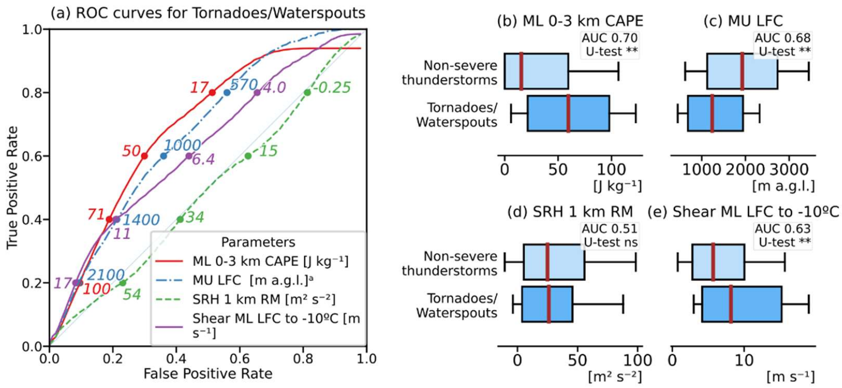

Figure 7: Convective parameters that best classify summer tornadoes against non-severe thunderstorms. (a) Receiver Operating Characteristic curves of selected parameters. The numerical values annotated correspond to the thresholds in each convective parameter that are exceeded ([a] not exceeded, for MU LFC) by 80%, 60%, 40% and 20 % of tornadoes (i.e., true positive rates). (b-e) Distributions of the parameters. Mann-Whitney U-tests evaluate if both distributions differ for various confidence levels (ns: below 0.95; **: 0.99). ML: mixed-layer parcel. MU: most-unstable parcel. LFC: level of free convection. SRH: storm-relative helicity. RM: right-mover motion.

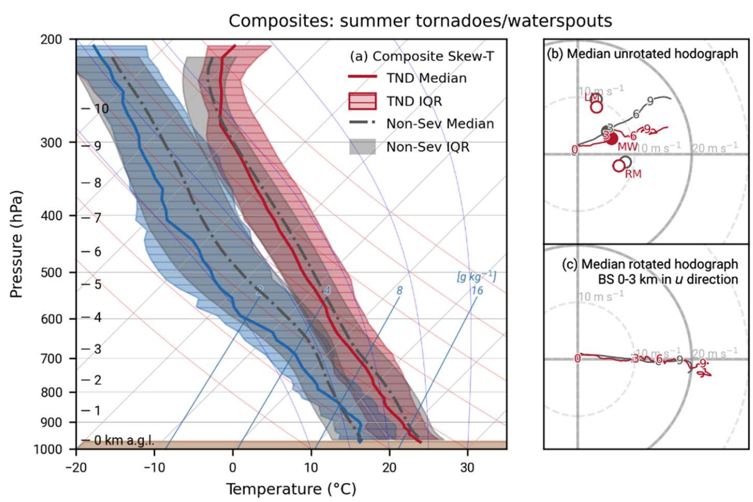

Figure 8: Composite profiles for summer tornadoes/waterspouts (TND; colored lines) and non-severe thunderstorms (Non-Sev; grey lines). (a) Composite skew-T diagram. (b) Median hodograph with 3, 6 and 9 km altitudes annotated, also including motion vectors of right-mover supercells (RM), left-mover supercells (LM) and the mean 0–6 km wind (MW). (c) Shear-relative composite hodograph, with the origin of single profiles shifted to the center of the hodograph and 0–3 km bulk shear (BS) aligned with the wind *u*-component (i.e., eastward).

https://doi.org/10.5194/egusphere-2026-5202
Preprint. Discussion started: 9 September 2026

3.2.2 Non-summer tornadoes

Despite non-summer TND having the greatest sample size among all the hazards, they remain the most challenging hazard to distinguish from non-severe environments, yielding ROC curves close to the no-skill 1:1 line (Supplementary Fig. S2) and a maximum AUC of only 0.62 (Table 7). This maximum AUC is shared by three parameters (K and Showalter indices, Lapse Rate 600-800 hPa), which moreover indicate less instability for TND than for non-severe environments. As in summer, the height of the level of free convection (LFC) remains lower for non-summer TND than for non-severe environments, but the overlap is greater as the LFC is found at lower altitudes than the rest of the year. Accordingly, moisture and temperature distributions in the composite skew-T diagram are highly similar between TND and non-severe environments (Supplementary Fig. S3a), as well as composite hodographs (Supplementary Fig. S3b,c), with only slightly increased shear over 9 km. However, the link of this finding with any known tornadogenesis mechanism is unclear, as most of them are associated with boundary layer processes (Nixon and Allen, 2022; Davies-Jones, 2015; Markowski and Richardson, 2010).

3.3 Large hail (summer)

The binary classification between summer large hail and non-severe thunderstorms scores a maximum AUC of 0.81 (Table 8), the highest across all hazards analyzed herein. Large hail is associated with very unstable and sheared environments compared to non-severe thunderstorms, as denoted by the top parcel-based and thermodynamic parameters (CAPE, $\Delta\theta_e$ and the Lifted Index), and the top kinematic parameter (wind shear, with mixed-layer effective shear outperforming the rest of shear formulations). ML CAPE contains several formulations that evaluate hail-sensitive layers, but these provide only slight improvements compared to simpler versions, as indicated by their AUC values (0.76, over -10ºC level, 0.74, hail growth layer; 0.75, whole profile), and the overlap in their ROC curves (Fig. 9a). Accordingly, the composite index WMAXSHEAR ranks as the best classifier, combining instability and shear.

Table 8: Ranking of the best convective parameters for classifying summer large hail and non-summer short-duration precipitation extremes (PRCP). The ratio of each hazard to non-severe thunderstorms is indicated with *n*. $\Delta\theta_e$: equivalent potential temperature deficits from mid-levels to surface. WMAXSHEAR: product of maximum updraft velocity and vertical shear. ML: mixed-layer parcel. MU: most-unstable parcel. LFC: level of free convection. [a] Higher values for non-severe thunderstorms.

Large hail, n = (112:14482)	AUC (σ)	PRCP, n = (105:12997)	AUC (σ)
ML Effective WMAXSHEAR	0.81(.02)	MU LFC Temperature	0.70(.03)
$\Delta\theta_e$	0.78(.02)	ML Mixing Ratio	0.70(.03)
Hail Size Index	0.78(.02)	Bunkers Right-Mover Motion	0.68(.03)[a]
ML CAPE over -10ºC	0.76(.03)	Precipitable Water	0.67(.03)
ML Lifted-Index	0.76(.02)	Freezing Level	0.66(.03)
Shear: Effective ML	0.75(.03)	Significant Hail Intensity Parameter	0.66(.03)
θ_e 0–1 km	0.72(.03)	Shear: ML LFC to -10ºC	0.65(.03)
Mean Storm Motion	0.68(.03)	Energy Helicity Index 0–3 km	0.65(.03)

Composite profiles (Fig. 10a) show that the elevated CAPE in large hail environments is a consequence of more moisture content at the boundary layers when compared to non-severe environments. This could be associated with easterly low-level winds (Fig. 10b) advecting moisture from the Western Mediterranean basin. Large hail hodographs are relatively long, nearly straight and only slightly backing (i.e., anti-clockwise curved) between 2 and 9 km (Fig. 10b,c).

https://doi.org/10.5194/egusphere-2026-5202
Preprint. Discussion started: 9 September 2026

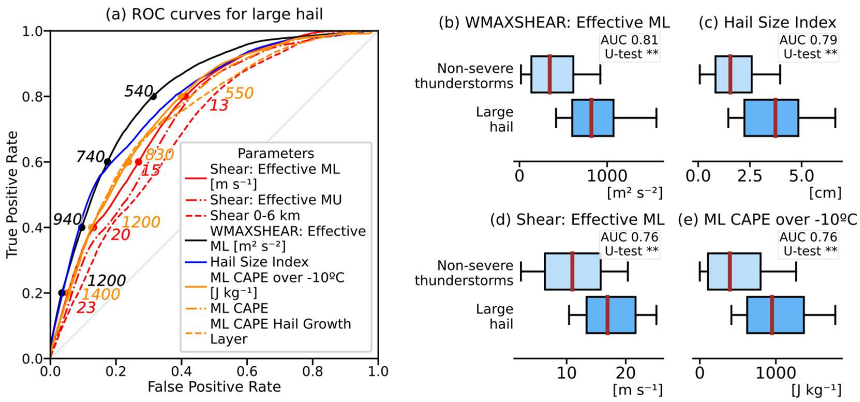

Figure 9: Convective parameters that best classify summer large hail against non-severe summer thunderstorms. (a) Receiver Operating Characteristic curves of selected parameters. The numerical values annotated correspond to the lower thresholds in each convective parameter that are exceeded by 80%, 60%, 40% and 20 % of hail environments (i.e., true positive rates). (b-e) Distributions of selected parameters. Mann-Whitney U-tests evaluate if both distributions differ for various confidence levels (ns: below 0.95; **: 0.99). ML: mixed-layer parcel. MU: most-unstable parcel. WMAXSHEAR: product of maximum updraft velocity and 0–6 km shear.

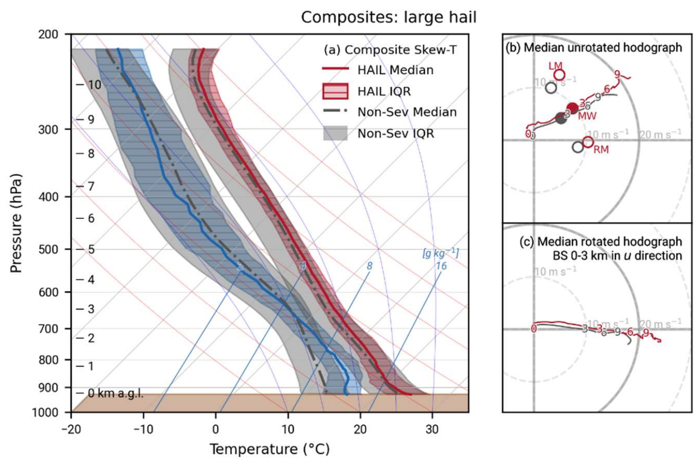

Figure 10: Composite profiles for summer large hail (HAIL; colored lines) and non-severe thunderstorms (Non-Sev; grey lines). (a) Composite skew-T. (b) Median hodograph with 3, 6 and 9 km altitudes annotated, also including motion vectors of right-mover supercells (RM), left-mover supercells (LM) and the mean 0–6 km wind (MW). (c) Shear-relative composite hodograph, with the origin of single profiles shifted to the center of the hodograph and 0–3 km bulk shear (BS) aligned with the wind *u*-component (i.e., eastward).

Physically, CAPE is related to strong updrafts allowing long periods of time for hail to grow before precipitating, and shear is related to storm morphology, with supercells being the exclusive morphology producing hail over 5 cm in diameter (Allen et al., 2020; Smith et al., 2012). Therefore, as herein, numerous studies have found both elevated CAPE and wind shear in hail environments (Wang et al., 2026; Calvo-Sancho et al., 2022; Taszarek et al., 2020; Púčik et al., 2015; Manzato, 2012; Groenemeijer and Van Delden, 2007; Kunz, 2007; López et al., 2001). Supercell indices achieved moderate large hail classification skill (Energy Helicity Index, Supercell Composite Parameter; both with AUC = 0.77), and the Hail Size Index scores a high AUC (0.78), but fails at estimating the minimum size of our sample (> 5 cm), even though it was derived from

https://doi.org/10.5194/egusphere-2026-5202
Preprint. Discussion started: 9 September 2026

European hail environments and has proven accurate in 10 cm hail case studies (Papavasileiou et al., 2022). Nevertheless, WMAXSHEAR, despite being a simpler index, outperformed these indices and other studies have also reported its skill (Taszarek et al., 2020; Dowdy et al., 2020; Czernecki et al., 2019).

Our WMAXSHEAR values (IQR = 700–1100 m^2 s^{-2}) are similar to the large hail environments in central of Europe (500–1000 m^2 s^{-2}; Taszarek et al. 2020) and Turkey (500–1000 m^2 s^{-2}; Yavuz et al., 2026). Similar ranges are also found during hailstorm days in Australia, although not exclusively for large hail (Warren et al., 2020). Regarding other of our top classifiers, effective shear provided the best distinction for hail severity in South America (Bechis et al., 2025), showing differences with other regions, as denoted by IQRs of 19–26 m s^{-1} (South America) and 13–22 m s^{-1} (Spain).

The reduced clockwise rotation of our composite hodographs (Fig. 10c) produces similar shapes to those documented for left-mover supercells producing large hail in Nixon and Allen (2022) and for the left-mover supercells in Feldmann et al. (2026), yet the shear of our sample is weaker by 2.5–5 m s^{-1} in the 0–3 km layer. However, our dataset does not contain any related information about right-mover or left-mover classification.

3.4 Short-duration precipitation extremes (non-summer)

The convective parameters that best classify between PRCP and non-severe thunderstorms are the mixing ratio of the mixed-layer parcel, precipitable water and the temperature of the level of free convection (Table 8). This indicates that PRCP environments contain more moisture and release their instability closer to the surface than non-severe environments (Fig. 11a,b,d). Regarding kinematic characteristics, PRCP environments support slower storm motions than non-severe environments, especially when storm motion is computed for right-mover supercells (Bunkers RM in Fig. 11c). Regarding composite indices, the Energy Helicity Index, resulted in a moderate classifier for PRCP (Table 8), as well as the Significant Hail Intensity Parameter.

Kinematic parameters formulated for left-mover motion or composite indices derived from them also appeared among the top parameters (Energy Helicity Index at various layers, AUC over 0.69), but their distribution is physically inconsistent, showing positive storm-relative helicity and streamwise vorticity, whereas anticyclonic rotation in left-mover motion should be associated with negative values. These positive values likely reflect easterly Mediterranean inflow advecting moisture (Fig. 12b), rather than left-mover true dynamics. For these reasons, left-mover kinematic parameters were excluded from Table 8.

The composite PRCP profiles in Fig. 12a show enhanced specific and relative humidity, mainly below 2 km and over 5 km altitudes, compared to non-severe profiles. Less markedly, temperature is also greater for PRCP profiles than for non-severe profiles (25th percentile), accordingly showing higher freezing levels for PRCP (Fig 11e). PRCP composite hodographs at 0–3 km exhibit a marked easterly component (Fig 12b) and clockwise curvature (Fig 12c), and weaker winds are observed in 9–12 km for PRCP, when PRCP and non-severe hodographs are compared (Fig. 12c).

Together these results align with typical heavy precipitation ingredients that increase precipitation efficiency (moisture availability and saturation), and allow persistent rainfall due to slow ground-relative motion (Burow et al., 2025; Markowski and Richardson, 2010; Doswell III et al., 1996). The parameter Bunkers RM, was also identified by Burow et al. (2025) as a relevant parameter in US flash flooding environments. The importance of this parameter, instead of the mean wind, in addition to clockwise rotating 0–3 km composite hodographs and moderate AUC of the Energy Helicity Index, could indicate supercell environments, which often produce extreme rainfall (Smith et al., 2012). Additionally, the weak wind over 9–12 km can support high-precipitation supercells by limiting hydrometeor dispersion (Rasmussen and Straka, 1998).

https://doi.org/10.5194/egusphere-2026-5202
Preprint. Discussion started: 9 September 2026

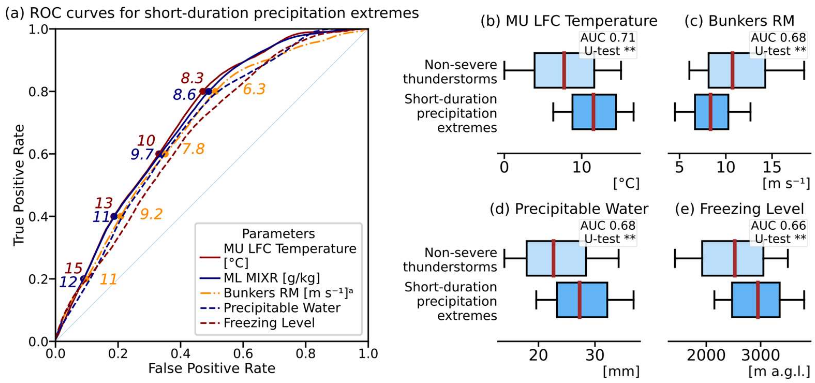

Figure 11: Convective parameters that best classify short-duration precipitation extremes against non-severe thunderstorms. (a) Receiver Operating Characteristic curves of selected parameters. The numerical values annotated correspond to the thresholds in each convective parameter that are exceeded ([a] not exceeded, for Bunkers RM) by 80%, 60%, 40% and 20 % of short-duration precipitation extremes (i.e., true positive rates). (b-e) Distributions of the parameters. Mann-Whitney U-tests evaluate if both distributions differ for various confidence levels (ns: below 0.95; **: 0.99). MU: most-unstable parcel. LFC: level of free convection. ML: mixed-layer parcel. RM: right-mover motion.

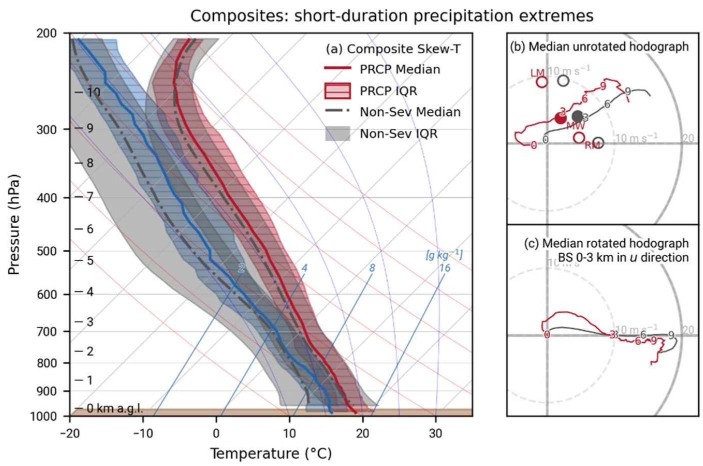

Figure 12: Composite profiles for non-summer short-duration precipitation extremes (PRCP; colored lines) and non-severe thunderstorms (Non-Sev; grey lines). (a) Composite skew-T. (b) Median hodograph with 3, 6 and 9 km altitudes annotated, also including motion vectors of right-mover supercells (RM), left-mover supercells (LM) and the mean 0–6 km wind (MW). (c) Shear-relative composite hodograph, with the origin of single profiles shifted to the center of the hodograph and 0–3 km bulk shear (BS) aligned with the wind *u*-component (i.e., eastward). Note the reduced scale in composite hodographs with respect to the previous composites.

3.5 Limitations

Although we have restricted to the same grids for each severe against non-severe comparison, in order to focus on physical environmental differences rather than climatological differences arising from reporting biases, we acknowledge that many localized severe weather events are unreported, thus contaminating our non-severe class. The development of automated severe convective weather detections from dense weather station networks will improve on this limitation (Azorin-Molina et al., 2025).

We also acknowledge that the relatively coarse resolution of ERA5 cannot explicitly resolve turbulence or mesoscale circulations, so boundary-layer temperature, CAPE or humidity evolve strongly controlled by the model parameterizations. Direct high-frequency and vertically resolved observations within the boundary layer are also comparatively sparse with respect to the many observations assimilated by ERA5 (Hersbach et al., 2020), which could contribute to the lower-tropospheric thermodynamic structure to remain model-dependent. CAPE extremes are usually underestimated in ERA5, which remains as a limitation in this research (Yiya et al., 2025; Wang et al., 2021; Taszarek et al., 2021b). Moreover, the simulated diurnal evolution of convective precipitation or deep convection has been found to peak too early, causing premature peaks in heating and precipitation (Liu et al., 2026; Dai, 2024). Therefore, it is possible that the predictive skill of many of the convective parameters tested herein is masked by these limitations, such as CAPE, for large hail, or kinematic parameters, for tornadoes. Upcoming km-scale reanalyses, such as IBERA, may improve the characterization of severe convective environments by better resolving extremes and overcoming the limitations imposed by ERA5's coarse resolution and parameterization schemes.

4. Conclusions

This research examined the atmospheric precursor environments of different hazards associated with severe convection in Spain, including downbursts, large hail, short-duration precipitation extremes and tornadoes/waterspouts. Our objective was to identify the key environmental differences between these severe and non-severe thunderstorms, in terms of convective parameters. To construct our samples, we combined ERA5, cloud-to-ground lightning flashes and public severe weather reports. We further separated the dataset into summer and non-summer months to account for the distinct forcing mechanisms previously documented, particularly for downbursts. Using Receiver Operating Characteristic (ROC) curves and the Area Under the Curve (AUC) score, we identified the parameters with the highest distinguishing skill for each hazard, which are summarized below:

- Summer downbursts are primarily associated with elevated values of DCAPE (e.g., 57% of them exceed 1000 J kg^{-1}, but only 17% of non-severe thunderstorms) and of thermodynamic parameters, showing steep lapse rates in inverted-V profiles and elevated freezing levels. Their temperature profiles are notably warmer than non-severe thunderstorms. For close to lightning downbursts ($\lesssim$ 15 km), composite indexes (such as the Downburst Environment Index) show the best predictive skill, while DCAPE outperforms composite indexes in the more general case that includes downbursts far from lightning ($\lesssim$ 45 km) or not associated with them.
- Non-summer downbursts are more difficult to distinguish from non-severe thunderstorms than their summer counterparts. They are associated with relatively strong shear compared to non-severe thunderstorms (particularly up to the -10 ºC isotherm), but our shear is still weak compared to the High-Shear–Low-CAPE severe environments documented in regions other than Spain, which may be offset by the climatologically moderate values of DCAPE reported herein.
- Tornadoes and waterspouts remain difficult to distinguish from non-severe thunderstorms, consistent with previous studies. They are more easily distinguished in summer, showing greater 0–3 km CAPE and lower level of free convection, indicatives of the stretching of pre-existent vorticity.
- Large hail occurs mainly in summer and is associated with greater instability and wind shear than for non-severe thunderstorms, highlighting the WMAXSHEAR index. Using effective formulations for shear and WMAXSHEAR noticeable improves the distinguishing skill for large than using simpler versions, whereas hail-sensitive formulations of CAPE (such as CAPE over -10 ºC level) provide only small improvements.
- Short-duration precipitation extremes develop in environments with greater moisture content and saturation than non-

https://doi.org/10.5194/egusphere-2026-5202
Preprint. Discussion started: 9 September 2026

severe thunderstorms, resulting in lower levels of free convection and condensation. Right-mover motion emerges as a relevant kinematic parameter, indicating that slow and persistent storms support this hazard. The Energy Helicity Index arises as another key parameter, showing moderate signatures of supercell environments in short-duration precipitation extremes.

Convective parameters are a fundamental tool for diagnosing and researching severe convection. The results presented here offer a framework for identifying the parameters with the greatest predictive skill across four severe convective weather hazards, suitable for the Mediterranean basin, and with a methodology that can be applied elsewhere. Together with ROC curves and parameter distributions, this information offers a practical reference for forecasters in the identification of potential severe weather outbreaks, and for researchers by providing climatological proxies of severe convection. However, the moderate AUC values obtained highlight that non-severe environments overlap substantially with severe environments. Future research will explore the application of machine learning approaches, such as Random Forests, to generate probabilistic estimations of severe convective weather.

Data availability

The severe weather datasets used herein are available through SINOBAS portal (https://sinobas.aemet.es/), excepting large hail which can be requested to C. Calvo-Sancho and consists of an updated version of the Spanish Supercell Dataset available in Zenodo (https://doi.org/10.5281/zenodo.10257815). ERA5 reanalysis is available from the Copernicus Climate Change Service Climate Data Store (https://doi.org/10.24381/cds.bd0915c6, Hersbach et al., 2020).

Author contributions

A.B., C.C., N.P. and C.A. conceived the ideas and aims, and led writing. A.B. performed data analysis and investigation. A.M. provided lightning data. All co-authors contributed critically to the writing of the manuscript.

Competing interests

The authors declare that they have no conflict of interest.

Acknowledgments

AEMET is gratefully acknowledged for providing cloud-to-ground lightning observations and publicly available severe weather reports (SINOBAS). Copernicus is gratefully acknowledged for providing publicly available ERA5 data. During the preparation of this work, the authors used Artificial Intelligence (AI) tools to assist with debugging and optimizing code for data processing, and to support minor language editing and text compaction. After using this tool, the authors reviewed and edited the content as needed and take full responsibility for the content of the published article

Financial support

This work was supported by a PROMETEO grant (Ref. CIPROM/2023/38; DOWNBURST project) for research groups of excellence funded by the Valencian Regional Government (GVA). We also received support from the CSIC-LINCGLOBAL Ref. LINCG24042; and CSIC's PTI-Clima. A. Barrio-Martin acknowledges the grant awarded by the Spanish Research Council - JAE Intro (BDNS 753215 - BOE 19-04-2024). C. Calvo-Sancho acknowledges the support by the grant PID2023-146344OB-I00 (CONSCIENCE) funded by MICIU/AEI/10.13039/501100011033 and by "ERDF A way of making Europe", and the ECMWF Special Projects (SPESSANC). N. P. Plaza-Martín acknowledges the European Commission-NextGenerationEU (EU Regulation 2020/2094) for the support through the CSIC Momentum Programme: Digital Talent Development.

https://doi.org/10.5194/egusphere-2026-5202
Preprint. Discussion started: 9 September 2026

Conflicts of Interest

The authors declare no conflict of interest. The funding sponsors have no participation in the execution of the experiment, the decision to publish the results, nor the writing of the manuscript.

References

Allen, J. T., Giammanco, I. M., Kumjian, M. R., Jurgen Punge, H., Zhang, Q., Groenemeijer, P., Kunz, M., and Ortega, K.: Understanding Hail in the Earth System, Reviews of Geophysics, 58, e2019RG000665, https://doi.org/10.1029/2019RG000665, 2020.

Antonescu, B., Schultz, D. M., Holzer, A., and Groenemeijer, P.: Tornadoes in Europe: An Underestimated Threat, Bulletin of the American Meteorological Society, 98, 713–728, https://doi.org/10.1175/BAMS-D-16-0171.1, 2017.

Arús Dumenjo, J.: Reventones de tipo cálido en Cataluña, in: V Simposio Nacional de Predicción [CD-ROM], 2001.

Azorin-Molina, C.: Situación atmosférica de "heat burst" en la provincia de Alicante, Eria, 237–254, 2005.

Azorin-Molina, C., Calvo-Sancho, C., Martin-Barrio, A., Granell-Haro, F., Gomez-Reyes, J., Prein, A. F., Gonzalez-Aleman, J. J., Vicente-Serrano, S. M., McVicar, T. R., Chen, D., and others: The DOWNBURST MXO: a real-time downburst monitoring service in eastern Spain, Copernicus Meetings, 2025.

Battaglioli, F., Groenemeijer, P., Púčik, T., Taszarek, M., Ulbrich, U., and Rust, H.: Modeled Multidecadal Trends of Lightning and (Very) Large Hail in Europe and North America (1950–2021), Journal of Applied Meteorology and Climatology, 62, 1627–1653, https://doi.org/10.1175/JAMC-D-22-0195.1, 2023.

Battaglioli, F., Taszarek, M., Groenemeijer, P., Púčik, T., and Rädler, A.: Contrasting trends in very large hail events and related economic losses across the globe, Nat. Geosci., 19, 52–58, https://doi.org/10.1038/s41561-025-01868-0, 2026.

Bechis, H., Zanetti Ribeiro, B., Cancelada, M., Salio, P., Ruiz, J., Granato, A., and Saucedo, M.: Environments associated with hail and convectively generated damaging wind gusts in South America, Quarterly Journal of the Royal Meteorological Society, 151, e5029, https://doi.org/10.1002/qj.5029, 2025.

Brown, A. and Dowdy, A.: Severe convection-related winds in Australia and their associated environments, JSHESS, 71, 30–52, https://doi.org/10.1071/ES19052, 2021.

Burow, D., Kressler, K., and Searcy, Z.: On the Convective Environments, Modes, and Warning Verifications of Tornado- and Flash Flood-Warned Storms in the Southeast United States, Meteorological Applications, 32, e70062, https://doi.org/10.1002/met.70062, 2025.

Calvo-Sancho, C., Díaz-Fernández, J., Martín, Y., Bolgiani, P., Sastre, M., González-Alemán, J. J., Santos-Muñoz, D., Farrán, J. I., and Martín, M. L.: Supercell convective environments in Spain based on ERA5: hail and non-hail differences, Weather and Climate Dynamics, 3, 1021–1036, https://doi.org/10.5194/wcd-3-1021-2022, 2022.

Calvo-Sancho, C., Díaz-Fernández, J., González-Alemán, J. J., Halifa-Marín, A., Miglietta, M. M., Azorin-Molina, C., Prein, A. F., Montoro-Mendoza, A., Bolgiani, P., Morata, A., and Martín, M. L.: Human-induced climate change amplification on storm dynamics in Valencia's 2024 catastrophic flash flood, Nat Commun, 17, 1492, https://doi.org/10.1038/s41467-026-68929-9, 2026.

Caplan, S., Bedard Jr, A., and Decker, M.: The 700–500 mb lapse rate as an index of microburst probability: An application for thermodynamic profilers, Journal of Applied Meteorology and Climatology, 29, 680–687, 1990.

Clark, M. and Smart, D.: Supercell and Non-supercell Tornadoes in the United Kingdom and Ireland, in: Extreme Weather, 31–59, https://doi.org/10.1002/9781118949986.ch3, 2015.

Corfidi, S. F.: Cold Pools and MCS Propagation: Forecasting the Motion of Downwind-Developing MCSs, Weather and Forecasting, 18, 997–1017, https://doi.org/10.1175/1520-0434(2003)018%3C0997:CPAMPF%3E2.0.CO;2, 2003.

Czernecki, B., Taszarek, M., Marosz, M., Półrolniczak, M., Kolendowicz, L., Wyszogrodzki, A., and Szturc, J.: Application of machine learning to large hail prediction - The importance of radar reflectivity, lightning occurrence and convective parameters derived from ERA5, Atmospheric Research, 227, 249–262, https://doi.org/10.1016/j.atmosres.2019.05.010, 2019.

Dai, A.: The diurnal cycle from observations and ERA5 in precipitation, clouds, boundary layer height, buoyancy, and surface fluxes, Clim Dyn, 62, 5879–5908, https://doi.org/10.1007/s00382-024-07182-6, 2024.

Davies-Jones, R.: A review of supercell and tornado dynamics, Atmospheric Research, 158–159, 274–291, https://doi.org/10.1016/j.atmosres.2014.04.007, 2015.

Dimri, A. P., Chevuturi, A., Niyogi, D., Thayyen, R. J., Ray, K., Tripathi, S. N., Pandey, A. K., and Mohanty, U. C.: Cloudbursts in Indian Himalayas: A review, Earth-Science Reviews, 168, 1–23, https://doi.org/10.1016/j.earscirev.2017.03.006, 2017.

Doswell, C. A., Burgess, D. W., and others: Tornadoes and tornadic storms: A review of conceptual models, Geophysical Monograph-American Geophysical Union, 79, 161–161, 1993.

Doswell, C. A., Brooks, H. E., and Maddox, R. A.: Flash Flood Forecasting: An Ingredients-Based Methodology, Weather and Forecasting, 11, 560–581, https://doi.org/10.1175/1520-0434(1996)011%3C0560:FFFAIB%3E2.0.CO;2, 1996.

Doswell, C. A. and Schultz, D. M.: On the Use of Indices and Parameters in Forecasting Severe Storms, E-Journal of Severe Storms Meteorology, 1, 1–22, https://doi.org/10.55599/ejssm.v1i3.4, 2006.

https://doi.org/10.5194/egusphere-2026-5202
Preprint. Discussion started: 9 September 2026

Dowdy, A. J., Soderholm, J., Brook, J., Brown, A., and McGowan, H.: Quantifying Hail and Lightning Risk Factors Using Long-Term Observations Around Australia, Journal of Geophysical Research: Atmospheres, 125, 2020JD033101, https://doi.org/10.1029/2020JD033101, 2020.

Evans, J. S. and Doswell, C. A.: Examination of Derecho Environments Using Proximity Soundings, Weather and Forecasting, 16, 329–342, https://doi.org/10.1175/1520-0434(2001)016%3C0329:EODEUP%3E2.0.CO;2, 2001.

Feldmann, M., Beer, S., Zeeb, A. W., Brennan, K. P., Wilhelm, L., and Martius, O.: Left- and right-moving supercell dynamics, environments and hazards – today and in future, Weather and Climate Dynamics, 7, 615–632, https://doi.org/10.5194/wcd-7-615-2026, 2026.

Fery, L. and Faranda, D.: Analysing 23 years of warm-season derechos in France: a climatology and investigation of synoptic and environmental changes, Weather and Climate Dynamics, 5, 439–461, https://doi.org/10.5194/wcd-5-439-2024, 2024.

Fujita, T. T.: "The Downburst" – Microburst and Macroburst, Satellite and Mesometeorology Research Project (SMRP), Department of Geophysical Sciences, University of Chicago, National Center for Atmospheric Research (NCAR) Archives, 1985.

Gatzen, C.: Climatology and large-scale Dynamics of Derechos in Germany, PhD Thesis, Universität zu Köln, 2018.

Gayà, M.: Tornadoes and severe storms in Spain, Atmospheric Research, 100, 334–343, https://doi.org/10.1016/j.atmosres.2010.10.019, 2011.

Geerts, B.: Estimating Downburst-Related Maximum Surface Wind Speeds by Means of Proximity Soundings in New South Wales, Australia, Weather and Forecasting, 16, 261–269, https://doi.org/10.1175/1520-0434(2001)016%3C0261:EDRMSW%3E2.0.CO;2, 2001.

George, J. J.: Weather Forecasting for Aeronautics, Academic Press, London, 673 pp., 1960.

González-Alemán, J. J., Insua-Costa, D., Bazile, E., González-Herrero, S., Marcello Miglietta, M., Groenemeijer, P., and Donat, M. G.: Anthropogenic Warming Had a Crucial Role in Triggering the Historic and Destructive Mediterranean Derecho in Summer 2022, Bulletin of the American Meteorological Society, 104, E1526–E1532, https://doi.org/10.1175/BAMS-D-23-0119.1, 2023.

Groenemeijer, P. H. and van Delden, A.: Sounding-derived parameters associated with large hail and tornadoes in the Netherlands, Atmospheric Research, 83, 473–487, https://doi.org/10.1016/j.atmosres.2005.08.006, 2007.

Gropp, M. E. and Davenport, C. E.: The Impact of the Nocturnal Transition on the Lifetime and Evolution of Supercell Thunderstorms in the Great Plains, Weather and Forecasting, 33, 1045–1061, https://doi.org/10.1175/WAF-D-17-0150.1, 2018.

Hadavi, M., Sun, L., and Romanic, D.: Normalized insured losses caused by windstorms in Quebec and Ontario, Canada, in the period 2008–2021, International Journal of Disaster Risk Reduction, 80, 103222, https://doi.org/10.1016/j.ijdrr.2022.103222, 2022.

Hadavi, M. and Romanic, D.: Atmospheric conditions conducive to thunderstorms with downbursts in Canada and a downburst precursor parameter, Atmospheric Research, 305, 107428, https://doi.org/10.1016/j.atmosres.2024.107428, 2024a.

Hadavi, M. and Romanic, D.: Machine Learning Investigation of Downburst-Prone Environments in Canada, Journal of Applied Meteorology and Climatology, 63, 677–697, https://doi.org/10.1175/JAMC-D-23-0178.1, 2024b.

Hart, J. A. and Korotky, W.: The SHARP workstation v1.50 users guide., 1991.

Huang, Y., Sun, J., Zhang, Y., Ma, R., Yang, X., and Tian, F.: Initiation, organizational modes and environmental conditions of severe convective wind events during the warm season over North China, Sci. China Earth Sci., 67, 2876–2894, https://doi.org/10.1007/s11430-024-1386-9, 2024.

James, R. P. and Markowski, P. M.: A Numerical Investigation of the Effects of Dry Air Aloft on Deep Convection, Monthly Weather Review, 138, 140–161, https://doi.org/10.1175/2009MWR3018.1, 2010.

Kirshbaum, D. J., Adler, B., Kalthoff, N., Barthlott, C., and Serafin, S.: Moist Orographic Convection: Physical Mechanisms and Links to Surface-Exchange Processes, Atmosphere, 9, https://doi.org/10.3390/atmos9030080, 2018.

Kunz, M.: The skill of convective parameters and indices to predict isolated and severe thunderstorms, Natural Hazards and Earth System Sciences, 7, 327–342, https://doi.org/10.5194/nhess-7-327-2007, 2007.

Liu, Y., Wang, X., Liu, Y., Tang, S., and Miao, H.: A process-oriented analysis of the summertime diurnal cycle of precipitation and diabatic heating over China in three reanalyses, Atmospheric Chemistry and Physics, 26, 6763–6779, https://doi.org/10.5194/acp-26-6763-2026, 2026.

Llasat, M. C., Marcos, R., Turco, M., Gilabert, J., and Llasat-Botija, M.: Trends in flash flood events versus convective precipitation in the Mediterranean region: The case of Catalonia, Journal of Hydrology, 541, 24–37, https://doi.org/10.1016/j.jhydrol.2016.05.040, 2016.

Llasat, M. C., del Moral, A., Cortès, M., and Rigo, T.: Convective precipitation trends in the Spanish Mediterranean region, Atmospheric Research, 257, 105581, https://doi.org/10.1016/j.atmosres.2021.105581, 2021.

López, L., Marcos, J. L., Sánchez, J. L., Castro, A., and Fraile, R.: CAPE values and hailstorms on northwestern Spain, Atmospheric Research, 56, 147–160, https://doi.org/10.1016/S0169-8095(00)00095-8, 2001.

Manzato, A.: Hail in Northeast Italy: Climatology and Bivariate Analysis with the Sounding-Derived Indices, Journal of Applied Meteorology and Climatology, 51, 449–467, https://doi.org/10.1175/JAMC-D-10-05012.1, 2012.

Markowski, P. and Richardson, Y.: Mesoscale Meteorology in Midlatitudes, 1st ed., Wiley, https://doi.org/10.1002/9780470682104, 2010.

Martín, Y. and Calvo-Sancho, C.: Spanish Supercell Dataset - Hail, https://doi.org/10.5281/zenodo.10257815, 2023.

Martín, M. L., Calvo-Sancho, C., Taszarek, M., González-Alemán, J. J., Montoro-Mendoza, A., Díaz-Fernández, J., Bolgiani, P., Sastre, M., and Martín, Y.: Major Role of Marine Heatwave and Anthropogenic Climate Change on a Giant Hail Event in Spain, Geophysical Research Letters, 51, e2023GL107632, https://doi.org/10.1029/2023GL107632, 2024.

Melani, S., Pasi, F., Gozzini, B., and Ortolani, A.: A four year (2007–2010) analysis of long-lasting deep convective systems in the Mediterranean basin, Atmospheric Research, 123, 151–166, https://doi.org/10.1016/j.atmosres.2012.09.006, 2013.

Miller, R. C.: Notes on Analysis and Severe-Storm Forecasting Procedures of the Air Force Global Weather Central, Air Weather Service, Scott AFB, IL, 1972.

Nixon, C. J. and Allen, J. T.: Distinguishing between Hodographs of Severe Hail and Tornadoes, Weather and Forecasting, 37, 1761–1782, https://doi.org/10.1175/WAF-D-21-0136.1, 2022.

Nixon, C. J., Allen, J. T., and Taszarek, M.: Hodographs and Skew Ts of Hail-Producing Storms, Weather and Forecasting, 38, 2217–2236, https://doi.org/10.1175/WAF-D-23-0031.1, 2023.

Núñez Mora, J. Á., Riesco Martín, J., and Mora García, M. A.: Climatología de descargas eléctricas y de días de tormenta en España, Agencia Estatal de Meteorología, https://doi.org/10.31978/639-19-007-7, 2019.

Pacey, G. P., Schultz, D. M., and Garcia-Carreras, L.: Severe Convective Windstorms in Europe: Climatology, Preconvective Environments, and Convective Mode, Weather and Forecasting, 36, 237–252, https://doi.org/10.1175/WAF-D-20-0075.1, 2021.

Papavasileiou, G., Kotroni, V., Lagouvardos, K., and Giannaros, T. M.: Observational and numerical study of a giant hailstorm in Attica, Greece, on 4 October 2019, Atmospheric Research, 278, 106341, https://doi.org/10.1016/j.atmosres.2022.106341, 2022.

Pilguj, N., Surowiecki, A., Taszarek, M., and Piasecki, K.: Quasi-Linear Convective Systems and Derechos across Europe: ERA5 Convective Environments and Synoptic-Scale Patterns, Monthly Weather Review, 153, 2769–2791, https://doi.org/10.1175/MWR-D-25-0029.1, 2025.

Prein, A. F.: Thunderstorm straight line winds intensify with climate change, Nat. Clim. Chang., 13, 1353–1359, https://doi.org/10.1038/s41558-023-01852-9, 2023.

Púčik, T., Groenemeijer, P., Rýva, D., and Kolář, M.: Proximity Soundings of Severe and Nonsevere Thunderstorms in Central Europe, Monthly Weather Review, 143, 4805–4821, https://doi.org/10.1175/MWR-D-15-0104.1, 2015.

Púčik, T., Castellano, C., Groenemeijer, P., Kühne, T., Rädler, A. T., Antonescu, B., and Faust, E.: Large Hail Incidence and Its Economic and Societal Impacts across Europe, Monthly Weather Review, 147, 3901–3916, https://doi.org/10.1175/MWR-D-19-0204.1, 2019.

Rasmussen, E. N. and Straka, J. M.: Variations in Supercell Morphology. Part I: Observations of the Role of Upper-Level Storm-Relative Flow, Monthly Weather Review, 126, 2406–2421, https://doi.org/10.1175/1520-0493(1998)126%3C2406:VISMPI%3E2.0.CO;2, 1998.

Rodríguez, O. and Bech, J.: Tornadic environments in the Iberian Peninsula and the Balearic Islands based on ERA5 reanalysis, International Journal of Climatology, 41, E1959–E1979, https://doi.org/10.1002/joc.6825, 2021.

Schuster, S. S., Blong, R. J., Leigh, R. J., and McAneney, K. J.: Characteristics of the 14 April 1999 Sydney hailstorm based on ground observations, weather radar, insurance data and emergency calls, Natural Hazards and Earth System Sciences, 5, 613–620, https://doi.org/10.5194/nhess-5-613-2005, 2005.

Sherburn, K. D. and Parker, M. D.: Climatology and Ingredients of Significant Severe Convection in High-Shear, Low-CAPE Environments, Weather and Forecasting, 29, 854–877, https://doi.org/10.1175/WAF-D-13-00041.1, 2014.

Showalter, A. K.: A Stability Index for Thunderstorm Forecasting, Bulletin of the American Meteorological Society, 34, 250–252, https://doi.org/10.1175/1520-0477-34.6.250, 1953.

Smith, B. T., Thompson, R. L., Grams, J. S., Broyles, C., and Brooks, H. E.: Convective Modes for Significant Severe Thunderstorms in the Contiguous United States. Part I: Storm Classification and Climatology, Weather and Forecasting, 27, 1114–1135, https://doi.org/10.1175/WAF-D-11-00115.1, 2012.

Solari, G.: Thunderstorm Downbursts and Wind Loading of Structures: Progress and Prospect, Frontiers in Built Environment, Volume 6-2020, https://doi.org/10.3389/fbuil.2020.00063, 2020.

Srivastava, R. C.: A Model of Intense Downdrafts Driven by the Melting and Evaporation of Precipitation, Journal of Atmospheric Sciences, 44, 1752–1774, https://doi.org/10.1175/1520-0469(1987)044%3C1752:AMOIDD%3E2.0.CO;2, 1987.

Significant Hail Parameter (SHiP): https://www.spc.noaa.gov/exper/soundings/help/ship.html, last access: 1 March 2021.

Taszarek, M., Brooks, H. E., and Czernecki, B.: Sounding-Derived Parameters Associated with Convective Hazards in Europe, Monthly Weather Review, 145, 1511–1528, https://doi.org/10.1175/MWR-D-16-0384.1, 2017.

Taszarek, M., Allen, J. T., Púčik, T., Hoogewind, K. A., and Brooks, H. E.: Severe Convective Storms across Europe and the United States. Part II: ERA5 Environments Associated with Lightning, Large Hail, Severe Wind, and Tornadoes, Journal of Climate, 33, 10263–10286, https://doi.org/10.1175/JCLI-D-20-0346.1, 2020.

Taszarek, M., Pilguj, N., Allen, J. T., Gensini, V., Brooks, H. E., and Szuster, P.: Comparison of Convective Parameters Derived from ERA5 and MERRA-2 with Rawinsonde Data over Europe and North America, Journal of Climate, 34, 3211–3237, https://doi.org/10.1175/JCLI-D-20-0484.1, 2021a.

Taszarek, M., Allen, J. T., Marchio, M., and Brooks, H. E.: Global climatology and trends in convective environments from ERA5 and rawinsonde data, npj Climate and Atmospheric Science, 4, 35, https://doi.org/10.1038/s41612-021-00190-x, 2021b.

Thompson, R. L., Mead, C. M., and Edwards, R.: Effective Storm-Relative Helicity and Bulk Shear in Supercell Thunderstorm Environments, Weather and Forecasting, 22, 102–115, https://doi.org/10.1175/WAF969.1, 2007.

Tudurí, E. and Ramis, C.: The Environments of Significant Convective Events in the Western Mediterranean, Weather and Forecasting, 12, 294–306, https://doi.org/10.1175/1520-0434(1997)012%3C0294:TEOSCE%3E2.0.CO;2, 1997.

Wakimoto, R. M.: Forecasting Dry Microburst Activity over the High Plains, Monthly Weather Review, 113, 1131–1143, https://doi.org/10.1175/1520-0493(1985)113%3C1131:FDMAOT%3E2.0.CO;2, 1985.

Wakimoto, R. M. and Wilson, J. W.: Non-supercell Tornadoes, Monthly Weather Review, 117, 1113–1140, https://doi.org/10.1175/1520-0493(1989)117%3C1113:NST%3E2.0.CO;2, 1989.

Wakimoto, R. M.: Convectively Driven High Wind Events, in: Severe Convective Storms, edited by: Doswell, C. A., American Meteorological Society, Boston, MA, 255–298, https://doi.org/10.1007/978-1-935704-06-5_7, 2001.

Wang, S., Luo, Y., Wu, C., Chen, Y., Li, Q., and Wang, H.: Synoptic Background and Atmospheric Conditions for Hailstorms in Weining (Yunnan-Guizhou Plateau): Multi-Source Data Support and Machine Learning-Based Parameter Importance Ranking, Earth and Space Science, 13, e2025EA004850, https://doi.org/10.1029/2025EA004850, 2026.

Wang, Z., Franke, J. A., Luo, Z., and Moyer, E. J.: Reanalyses and a High-Resolution Model Fail to Capture the "High Tail" of CAPE Distributions, Journal of Climate, 34, 8699–8715, https://doi.org/10.1175/JCLI-D-20-0278.1, 2021.

Warren, R. A., Ramsay, H. A., Siems, S. T., Manton, M. J., Peter, J. R., Protat, A., and Pillalamarri, A.: Radar-based climatology of damaging hailstorms in Brisbane and Sydney, Australia, Quarterly Journal of the Royal Meteorological Society, 146, 505–530, https://doi.org/10.1002/qj.3693, 2020.

Xue, M., Zhao, K., Wang, M., Li, Z., and Zheng, Y.: Recent significant tornadoes in China, Advances in Atmospheric Sciences, 33, 1209–1217, https://doi.org/10.1007/s00376-016-6005-2, 2016.

Yavuz, V., Kara, Y., Temiz, C., and Deniz, A.: Long-Term Statistical Analysis of Hail Events and ERA5-Based Convective Environments Across Türkiye, Pure and Applied Geophysics, 183, 1979–1998, https://doi.org/10.1007/s00024-026-03922-3, 2026.

Yiya Y., Na H., Xiaoding Y., Junjie Z., and Luyang X.: Comparison of Summer Convective Parameters Calculated from ERA5 Reanalysis Data and Soundings in Beijing, yyqxxb, 36, 705–718, https://doi.org/10.11898/1001-7313.20250606, 2025.